


Article

# Weathering of Ophiolite Remnant and Formation of Ni Laterite in a Strong Uplifted Tectonic Region (Yuanjiang, Southwest China)

Wei Fu <sup>1,2,\*</sup> , Yangyang Feng <sup>1</sup>, Peng Luo <sup>1</sup>, Yinmeng Zhang <sup>1</sup>, Xiaorong Huang <sup>1</sup>, Xiangwei Zeng <sup>1</sup>, Qian Cai <sup>1</sup> and Yongzhang Zhou <sup>2</sup>

<sup>1</sup> Guangxi Key Laboratory of Hidden Metallic Ore Deposits Exploration, Guilin University of Technology, Guilin 541004, China; fengyangyang1021@163.com (Y.F.); pluo765@163.com (P.L.); zhangyinmeng9312@163.com (Y.Z.); hxrong30@163.com (X.H.); samwayzeng@163.com (X.Z.); caiqian7788@163.com (Q.C.)

<sup>2</sup> Center for Earth Environment & Resources, Sun Yat-sen University, Guangzhou 510275, China; zhouyz@sysu.edu.cn

\* Correspondence: fuwei@glut.edu.cn; Tel./Fax: +86-0773-5897019

Received: 30 November 2018; Accepted: 10 January 2019; Published: 16 January 2019



**Abstract:** The Yuanjiang Ni deposit in southwestern margin of the Yunnan Plateau is the only economically important lateritic Ni deposit in China. It contains 21.2 Mt ore with an average grade of 1.05 wt % Ni and has been recognized as the second largest Ni producer in China following the Jinchuan super-large magmatic Ni–Cu deposit. This Ni deposit is hosted within the lateritic regolith derived from serpentinite within the regional Paleo-Tethyan Ophiolite remnants. Local landscape controls the distribution of the Ni mineralized regolith, and spatially it is characterized by developing on several stepped planation surfaces. Three types of lateritic Ni ores are identified based on Ni-hosting minerals, namely oxide ore, oxide-silicate mixed ore and silicate ore. In the dominant silicate ore, two phyllosilicate minerals (serpentine and talc) are the Ni-host minerals. Their Ni compositions, however, are remarkably different. Serpentine (0.34–1.2 wt % Ni) has a higher Ni concentration than talc (0.18–0.26 wt % Ni), indicating that the serpentine is more significantly enriched in Ni during weathering process compared to talc. This explains why talc veining reduces Ni grade. The geochemical index (S/SAF value = 0.33–0.81, UMIA values = 17–60) indicates that the serpentinite-derived regolith has experienced, at least, weak to moderate lateritization. Based on several lines of paleoclimate evidence, the history of lateritization at Yuanjiang area probably dates to the Oligocene-Miocene boundary and has extended to the present. With a hydrology-controlled lateritization process ongoing, continuous operation of Ni migration from the serpentinite-forming minerals to weathered minerals (goethite and serpentine) gave rise to the development of three types of Ni ore in the regolith. Notably, the formation and preservation of the Yuanjiang lateritic Ni deposit has been strongly impacted by regional multi-staged tectonic uplift during the development of Yunnan Plateau. This active tectonic setting has promoted weathering of serpentinite and supergene Ni enrichment, but is also responsible for its partial erosion.

**Keywords:** lateritic Ni deposit; lateritization process; serpentine; paleoclimate; tectonic uplift; China

## 1. Introduction

Chemical weathering of ultramafic rocks has produced numerous lateritic profiles and associated Ni deposits, as best illustrated by those in New Caledonia, Cuba, Philippines, Indonesia, Colombia, Australia, and Brazil [1,2]. These deposits, commonly termed as lateritic Ni deposits, account for 60%–70% of the world's nickel resource and nearly 60% of the annual global nickel production [3].

They are mostly situated in equatorial latitudes characterized by warm and humid tropical climate at present or ancient time. Genetically, it is associated with obducted ophiolite complexes in accretionary belts or komatiites and layered ultramafic rocks in stable cratonic blocks [4,5]. In the last two decades, lateritic Ni deposit have received increasing attention in both the economic geology and exploration communities [6–18], largely due to the development of metallurgical technology for lateritic Ni ores and the shortage of sulfide Ni resources [19]. Ni laterites are also considered worthy targets for critical metals (REE, Sc, PGE, etc.) exploration [20].

Previous studies have significantly advanced our understanding in the nature and origin of lateritic Ni deposits: (1) Based on the dominant Ni-hosting minerals, lateritic Ni deposits can be divided into the oxides, hydrous Mg silicates and clay silicates subtypes. Such a subdivision is of economic importance in terms of resource evaluation and mineral processing [3,6]. (2) Large vertical variation in mineralogy and geochemistry of Ni-rich laterite profiles record the complex lateritization history of ultramafic rocks [7,21]. (3) Supergene Ni enrichment (in some case accompanied by Co enrichment) can be summarized as a eluviation-illuviation effect, which generated a significant change in Ni concentration, Ni speciation and even Ni isotope in the rock–regolith system [3,22–24]. (4) Formation of Ni-rich secondary minerals at atmospheric pressure and temperature is ascribed to a series of supergene processes regulated by water–rock interaction with lateritization ongoing, including sorption, substitution, dissolution/precipitation, etc. [18,21,25]. (5) Mode of occurrence of the lateritic Ni deposits are controlled by a combination of geological, climatic, topographic, and hydrologic parameters [4,5,7], especially the importance of topographic-hydrologic controlling on its ore grade is highly concerned in recent studies [25–27]. (6) Some lateritic deposits may have been products of multiphase chemical weathering, and their preservation reflects balance between weathering and erosion [3,15,21]. Despite the general understanding in the formation and genesis of lateritic Ni deposits, details on processes and evolution of supergene Ni enrichment remain enigmatic due to the complex parent rock lithologies and local environmental conditions.

Several lateritic Ni deposits have been discovered in China, including the Yuanjiang [28], Malipo deposits in Yunnan Province and the Chaiziyuan deposit in Sichuan Province [29], which are tectonically located along the Tethyan ophiolite belts in Southwest China. These lateritic Ni deposits have been explored and mined for more than 40 years, but little research has been published. In this paper, we present the geological, mineralogical and geochemical data of the Yuanjiang deposit. The results are used to provide insights into the formation and evolution of the Yuanjiang deposit, which in turn help build a genetic model in the context of regional geological evolution.

## 2. Geological and Geographical Setting

The Yuanjiang deposit is located in the southwestern portion of Yuanjiang county, Yunnan Province, Southwest China (Figure 1a). Tectonically, it is within the Ailaoshan suture, which marks the closure of the Ailaoshan ocean basin and subsequent late Triassic collision of the Yangtze plate in the northeast and the Simao-Indosinian plate in the southwest [30,31]. Ultramafic bodies occur as isolated exposures in this tectonic belt, and they have been interpreted to be a part of the Ailaoshan ophiolite complex that extends for >300 km along a NW–SE strike [32]. The main ultramafic bodies include, from north to south, Bailadu, Jinchang, Anding, Longtan, Mengli and Midi (Figure 1b). These ultramafic bodies are lithologically dominated by lherzolite, harzburgite, or peridotite, with variable serpentine alteration [33].

Other exposed geological units include the Permian to Triassic marine sedimentary rocks, the Ailaoshan metamorphic belt and unconsolidated Quaternary sediments [34]. The Permian to Triassic sequences are mainly composed of sandstones, conglomerates, mudstones, and intercalated shales, which are variably intruded by the ultramafic bodies and subjected to sub greenschist facies metamorphism in places where they were intruded by the intrusive rocks. The Ailaoshan metamorphic belt occurs to the north of the ophiolite complex and consists of granitic gneiss, quartz-feldspar-biotite gneiss, quartz-mica schist and banded marble. Quaternary sediments are limited to some terrestrial basins or low relief upland landscapes and consist of unconsolidated sandstones and conglomerates.

The mining area is situated near the Tropic of Cancer (23.5° N) and currently has a subtropical climate, with an average yearly precipitation more than 1600 mm and a mean annual temperature of 18–20 °C. Local geomorphology is a part of the Yunnan plateau on the southeastern margin of the Tibetan Plateau, consisting of hummocky mountains, ridges and intermountain basins. At least six planation surfaces, which are distributed in a vertical extent of ca. 400 m between 1700 and 2100 m, have been identified within the ore district and surrounding areas. Such a stepped topographic feature has also been reported in other areas of the Yunnan plateau and is interpreted to reflect a staged uplift and episodic erosion history [35,36]. The planation surfaces are variably mantled by lateritic profiles with a few tens of meters thickness, and the lateritic regolith is commonly disconnected by local drainage incision.

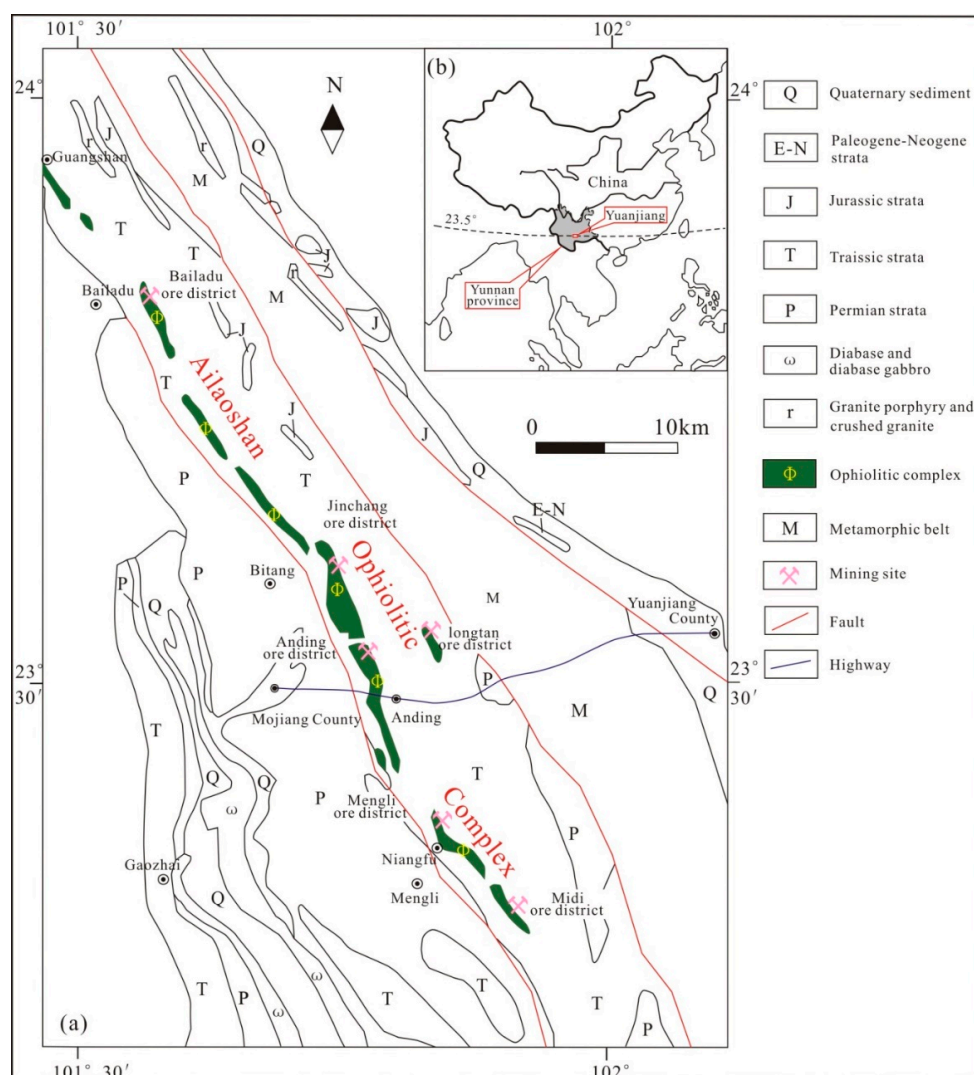


**Figure 1.** Simplified geological map of the Yuanjiang region, Yunnan Province, SW China, showing the location (a) and main geological context (b) of the study area.

### 3. Geology of the Yuanjiang Deposit and Profile Description

The Yuanjiang deposit is the largest lateritic Ni deposit in China with proven reserves of 21.2 Mt at > 1.05 wt % Ni, and it also represents the second largest Ni producer in China following the Jinchuan super-large magmatic Ni–Cu deposit. This deposit contains six ore districts: Bailadu, Jinchang, Anding, Longtan, Mengli and Midi. These ore districts are scattered along the Ailaoshan ophiolite belt and are spatially related to different ophiolite remnants. Among them, the Anding and Jinchang ore districts

are the main mining parts of the whole deposit. The Jinchang ore district is located within the outcrop area of the Jinchang ultramafic body, which is 15.6 km long and 0.4–1.93 km wide. The Anding ore district is located to the southeast of the Jinchang ore district, where the Anding ultramafic body is exposed in an area 7.2 km long and 0.3–0.8 km wide. Approximately 20–50% of the ultramafic bodies are covered with regolith, which provide the host of lateritic Ni ore.

Nickel mineralized lateritic profiles are mainly distributed in the third (Figure 2a) and fourth planation surfaces at altitudes of 1850–1860 m and 1920–1940 m, respectively. They have variable thickness, mostly ranging from 6 to 13 m but locally exceeding 40 m (Figure 3a). The thickness of weathering profiles reflects a combined effect of multiple factors such as lithologies of parent rocks, fracture intensity, local geomorphological features, and recent erosion. Weathering profiles developed on flat hilltops and low-lying plains are generally thicker than those on steep slopes and high-elevation ridges. In areas where fractures or joints are particularly developed, weathering profiles may become unusually thick due to preferential downward propagation of weathering front along more permeable zones. Weathering profiles on high-elevation ridges and steep slopes have been significantly eroded, with the bedrock or saprolite exposed at the present surface (Figure 2h). The parent lithologies are dominated by massive serpentinite (Figure 2i), which are locally overprinted with talc and calcite veins.

The lateritic weathering profile is typically divided into two main horizons according to variations in color, texture and mineral composition: the saprolitic zone at lower part and the limonitic zone at upper part (Figure 3b). The saprolite is most developed in flat planation surfaces with thickness from 6 to 20 m. It is overlying the serpentinite and generally has an irregular and transitional contact. This zone is typically yellowish-brown, grayish-yellow or grayish-green in color and shows porous, friable and heterogranular textures (Figure 2e). Many serpentinite relicts may occur at the lower part of saprolite (Figure 2g), and original parent rock textures are partly preserved as well. The silicate minerals (serpentine and talc) are the dominant components of the saprolite. More specifically, two types of saprolite can be further discriminated in this zone, termed as the green saprolite occurring in the lower part and the brown saprolite occurring in the upper part. The brown-saprolite contains a small amount of Fe-oxyhydroxides and its texture seems earthier compared to the green saprolite. The limonitic zone, mostly 2–10 m in thickness, is developed immediately above the saprolite. The contact between the two zones is clear and can be readily recognized by their contrasting color, texture and mineral compositions (Figure 2b). It is typically brownish-red to brownish-yellow, soft, porous, and fine-grained (Figure 2c). Original parent rock textures have almost disappeared in this position. The mineralogy of this horizon is dominated by Fe-oxyhydroxides with minor silicate or heavy minerals. Two sub-units can be further divided, lower brown limonite and upper red limonite, which reflect their somewhat different mineral or chemical compositions, as described below. In addition, small amount of hard ferruginous concretions, with diameters of a few to several tens of mm, can be observed within the limonite locally. To the top of the profile, the limonitic zone is variably covered by alluvial or other transported deposits. This cover is yellow-brown and mainly composed of sandy clay, with scattered gravels of ultramafic rocks or clastic rocks from adjacent sedimentary sequence.

Nickel mineralization is mainly concentrated in the lower part of the limonitic zone and the middle to upper part of the saprolite. According to mine geologists, the Ni ore can be generally sub-divided into three types based on the relative concentrations of Fe and Mg:

- I: Ferruginous ore (Figure 2d) in the brown limonite: 0.5–1.3 wt % Ni; <10 wt % Mg; ~24 wt % Fe.
- II: Ferruginous-magnesian ore (Figure 2d) in the brown saprolite: 0.5–1.6 wt % Ni; 10–20 wt % Mg; 11–13% wt % Fe.
- III: Magnesian ore (Figure 2e) in the green saprolite: 0.2–1.3 wt % Ni; >20 wt % Mg; 8–11 wt % Fe.

The magnesian ores account for the majority of total reserve and production. According to the general classification for lateritic Ni ore [4], the ferruginous and magnesian ores in the Yuanjiang deposit broadly correspond to the oxide and silicate ores, respectively, with the ferruginous-magnesian ore is mixed oxide-silicate ore.



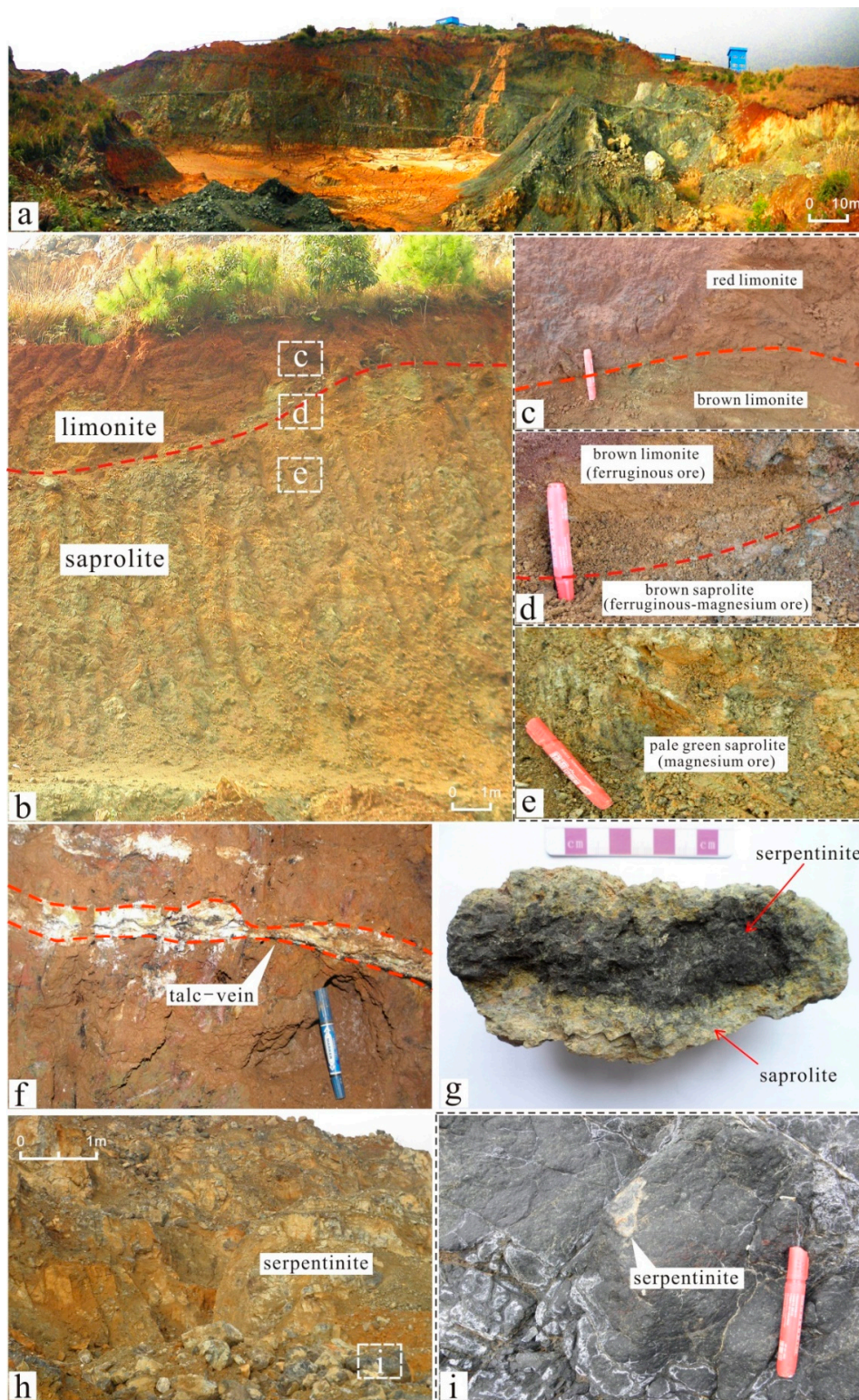


**Figure 2.** Macrophotographs of the lateritic Ni profile at the Yuanjiang area, showing its field geological characteristics: (a) lateritic regolith at the III-level denudation plane; (b) a typical lateritic Ni profile showing the divided regolith units; (c) the boundary of red limonite and brown limonite; (d) the boundary of brown limonite and brown saprolite; (e) the pale green saprolite developed in the middle and lower part of the profile; (f) the residual talc-vein in the saprolite horizon; (g) a typical rocky saprolite showing a black bedrock core surrounded by green saprolite; (h) outcrop of the bedrock exposed by mining; and (i) fresh serpentinite in the bedrock.

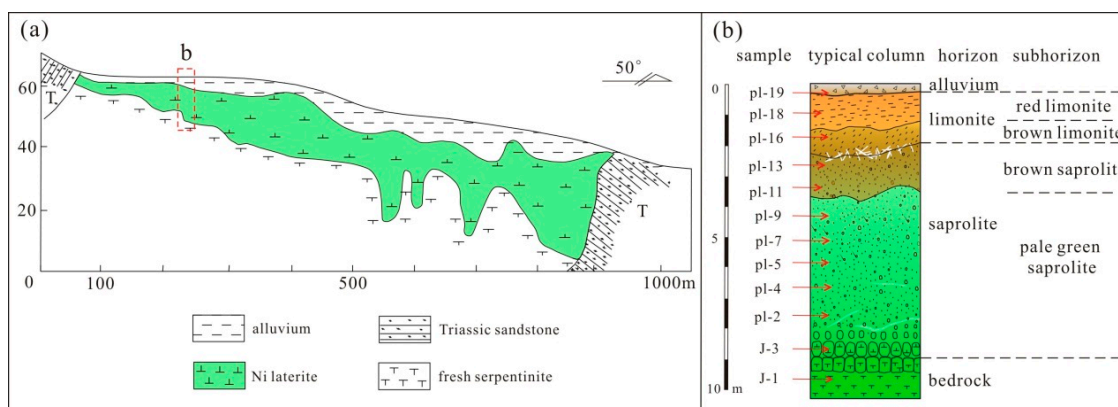


**Figure 3.** The typical long cross-section (a) and vertical column (b) of the Ni laterite profile from the study site at the Yuanjiang area, including the location of the samples.

Overall, the Yuanjiang Ni-bearing lateritic profile is characterized by a thick saprolite horizon as the main regolith unit and an abundance of silicate ore as the main type of the Ni ore. This is similar to other hydrous Mg silicate lateritic Ni deposits, for example the Sorowako deposit in Indonesia [37], the Cerro Matoso S. A. deposit in Colombia [6], and other cases worldwide (Figure 4). Therefore, the Yuanjiang deposit can be considered as the hydrous Mg silicate type. Comparatively, the ore grade of the Yuanjiang deposit (mean 1.05 wt % Ni) is relatively lower than most hydrous Mg silicate Ni deposits (mean 1.53 wt % Ni), possibly because of the absence of high grade garnierite ore. The so-called garnierite ore is defined as a mixture of neoformed hydrous Mg–Ni silicates with distinctive green color, poor crystallinity and high Ni contents (up to 30–40 wt % Ni), as reported in many hydrous Mg silicate type Ni laterites [10,23,24,38]. However, the garnierite ore does not always exist in the hydrous Mg silicate Ni deposits, such as in the case of Riddle in Oregon, USA [39].

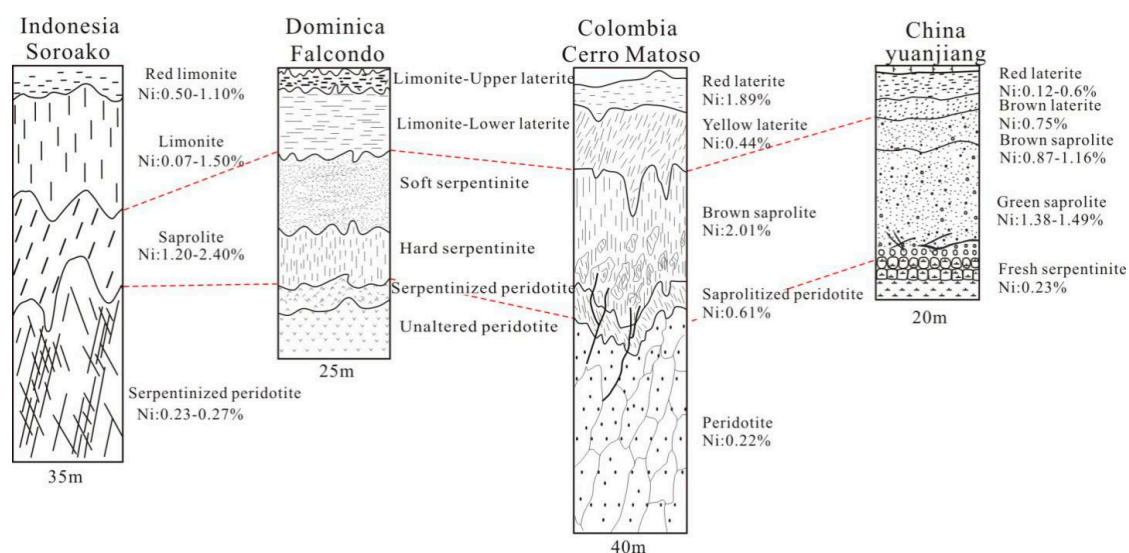


**Figure 4.** Comparison of the Yuanjiang lateritic Ni profile with other typical silicate-type lateritic Ni profiles around the world, including the Soroako profile in Indonesia [40], Falcondo profile in Dominica [9,41], and Cerro Matoso profile in Colombia [6]. The dotted lines show the boundaries of the saprolite horizons hosted silicate ore within the lateritic profiles from different sites.

#### 4. Samples and Analytical Methods

One ideal site for detailed regolith profile study was selected within the main mining area of the Jinchang ore district. It is a continuous and thick section with a vertical extent of ca. 10 m (Figure 3a,b), reflecting the most representative features of the lateritic Ni profile in the region. Sampling was



conducted orderly from the fresh parent rock through the saprolite zone and limonite zone to the alluvial cover, as shown in Figure 3b. To ensure the representativeness of samples, all samples were collected by similar volume standard of 1000 cm<sup>3</sup>. Totally, 11 samples were collected for laboratory analyses, including one parent rock sample (sample J-1), 7 saprolite samples (samples J-3, P<sub>1</sub>-2, P<sub>1</sub>-5, P<sub>1</sub>-7, P<sub>1</sub>-9, P<sub>1</sub>-11 and P<sub>1</sub>-13), 2 limonitic samples (P<sub>1</sub>-16 and P<sub>1</sub>-18), and an alluvial sample (P<sub>1</sub>-19).

Prior to laboratory analyses, all samples were naturally dried, and then each sample was divided into several parts for different examinations. Original samples were used to analyze the bulk density. Standard double-polished thin sections were prepared for examinations using optical microscopy and electron microprobe analysis (EMPA). Powdered samples of 200 meshes were analyzed using X-ray diffraction (XRD) and bulk geochemical techniques.

The bulk density was determined applying the traditional wax sealing method. Firstly, small fragment of the hard rock or regolith sample were picked and weighed using electronic scale. Next, the sample was dipped into melted max at 80 °C for several minutes, making the surface of sample totally coated by max. Then, the wax-sealed sample was put into the measuring cylinder with water to get the volume data of the sample. Finally the bulk density was calculated as a function of weight and volume.

X-ray diffraction data were acquired using a Philips X' Pert MPD diffractometer equipped with a Cu target tube, working at 40 kV and 40 mA. The range of 2θ scanning was from 5° to 80°. Scan step and step duration were 0.05° and 3 s, respectively. Standard grinding and mounting of the sample were performed prior to XRD analysis.

Whole-rock samples for geochemical analyses were dried at 70 °C and then crushed and powdered in an agate mill. The powder was further heated at 105 °C to remove adsorbed water before analysis. Major elements (Si, Al, Ca, Fe, K, Mg, Mn, Na, Ni and P) were measured using a Rigaku X-ray fluorescence spectrometer (XRF). The accuracies of the XRF analyses are estimated to be ~2% (relative) for elements oxides with concentrations greater than 2 wt %, and ~5% for those present in concentrations greater than 0.1 wt %. The detection limits for the major elements are generally better than 30 mg/kg. For trace elements (Sc, Ti, V, Co, Cu, Zn, Ge, Rb, Sr, Y, Zr, Nb, Cs, Ba, Hf, Ta, Pb, Th and U) analysis, the samples were first digested by an HNO<sub>3</sub> + HF acid mixture in high-pressure bombs, and then measured using a Perkin-Elmer Elan 6000 ICP-MS with detection limits of about 10 µg/kg in solid samples for trace elements. The precision of ICP-MS analyses is estimated to be better than 5% (relative) for most trace elements with concentrations greater than 10 mg/kg and ~10% for elements less than 10 mg/kg.

Electron microprobe analyses were made using a JXA-8230 electron microprobe attached with a wavelength dispersive system. The measurement conditions were 20 kV accelerating voltage, 15 nA probe current, and 2 µm beam diameter. Calibrations were performed using natural and synthetic reference materials: forsterite (Mg, Fe, and Si), anorthite (Ca), albite (Na and, Al), chromite (Cr), phlogopite (K), rutile (Ti), NiO (Ni), CoO (Co), and MnO (Mn). Back-scattered electron images and elemental X-ray maps of Fe, Mg, and Ni were made at 15 keV and 10 nA.

Some laboratory work, including petrography, XRD and EMPA, was conducted in the Key Laboratory of the Guangxi Hidden Metallic Ore Deposits Exploration in China, and the rest (whole-rock geochemical analyses) was carried out in the Key Laboratory of Geochronology and Geochemistry, Chinese Academy of Sciences.

## 5. Results

### 5.1. Bulk Density and Mineralogy

Bulk density is an important physical parameter of the lateritic Ni ore as it is required for industrial utilization and ore genesis study. In the profile studied, the bulk density decreases from 2.455 g/cm<sup>3</sup> in the fresh serpentinite to 1.196–1.672 g/cm<sup>3</sup> in the saprolite and 0.851–1.094 g/cm<sup>3</sup> in the limonite. These values are comparable to other reported examples of ultramafic rocks regolith [42].

Petrographic observations show that the parent rock is mineralogically dominated by serpentine, which is characterized by a fibrous or laminar crystal shape with pale to white color under transmitted-light microscopy (Figure 5a,b). Minor primary minerals include pyroxene (mainly clinopyroxene), magnetite and olivine. Most of them are isolated or enveloped by serpentine veins, forming a typical mesh-like structure (Figure 5a). The amounts of pyroxene and olivine account for less than 10% of total primary minerals, indicating strong serpentinization of the parent rocks. Fine veins of talc are locally observed, which are filled in the microfracture and crosscut with the serpentine aggregates (Figure 5b). Trace amounts of chromite are also presented and included in serpentine aggregates.

Results of XRD reveal that serpentine remains the most abundant mineral phase at the lower part of saprolite, which is reflected by a strong peak at 7.29 Å in the XRD pattern (Figure 6). This suggests that most of the serpentines of parent rock were retained during weathering. Other components including talc and hematite are also identified by XRD in the samples from the lower part of saprolite. Pyroxene, occurring as a relict phase surrounded by the serpentine aggregates (Figure 5c), is also identified under the microscope, but it is relative rare in the saprolite. Olivine is absolutely absent in both the petrographic observations and XRD patterns. This may indicate that almost all of olivine and the majority of pyroxene were altered in the first stage of weathering. At the upper part of the saprolite, the mineralogical composition is not substantially changed relative to its lower analog, but there is a trend of increasing in the mineral abundance of hematite and decreasing serpentine, as reflected by petrographic observations (Figure 5d).

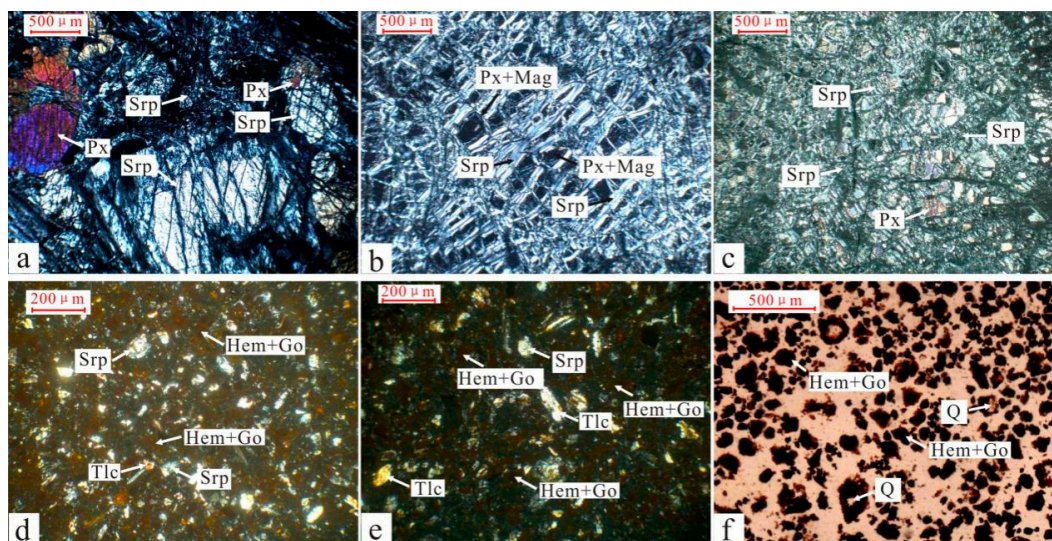


**Figure 5.** Microphotographs of the studied samples at the Yuanjiang lateritic Ni profile, showing its mineralogical composition and textures: (a) the dominant primary minerals in the bedrock including serpentine and pyroxene; (b) a typical mesh structure forming by serpentine, pyroxene and magnetite; (c) a small amount of residual pyroxene in the serpentine dominant saprolite horizon; (d) hematite and goethite appear in the brown saprolite dominated by serpentine; (e) hematite and goethite occur largely coexisting with a small amount of residual talc and serpentine together in the limonite horizon; and (f) concretions of hematite and goethite and quartz grains in the uppermost of the limonite horizon. Abbreviations: Go, goethite; Hem, hematite; Srp, serpentine; Qv, quartz; Px, pyroxene; Tlc, talc; Mag, magnetite.

The limonitic zone is dominated by cryptocrystalline to fine grained Fe oxides and hydroxides, mostly goethite and hematite (Figure 5a). Goethite and hematite have considerable overlap in XRD patterns, but they can be differentiated by the presence of a characteristic peak at 4.17 Å (goethite) and at 2.7 Å (hematite). Under transmitted- and reflected-light, goethite appeared yellowish, whereas hematite retained its reddish-brown color. Talc is still well preserved (Figure 5e) in the limonitic



zone, as shown by its characteristic peak at 9.35 Å, whereas serpentine has nearly disappeared. This observation indicates that talc is present from parent rock through saprolite horizon to limonite horizon, showing more robust status than serpentine in the weathered products. Quartz is also presented in the upmost horizon (Figure 5f), and the unusual appearance of this mineral may reflect an external input, because it seems that there are no rational genetic associations between quartz and primary minerals or those of secondary weathered minerals.

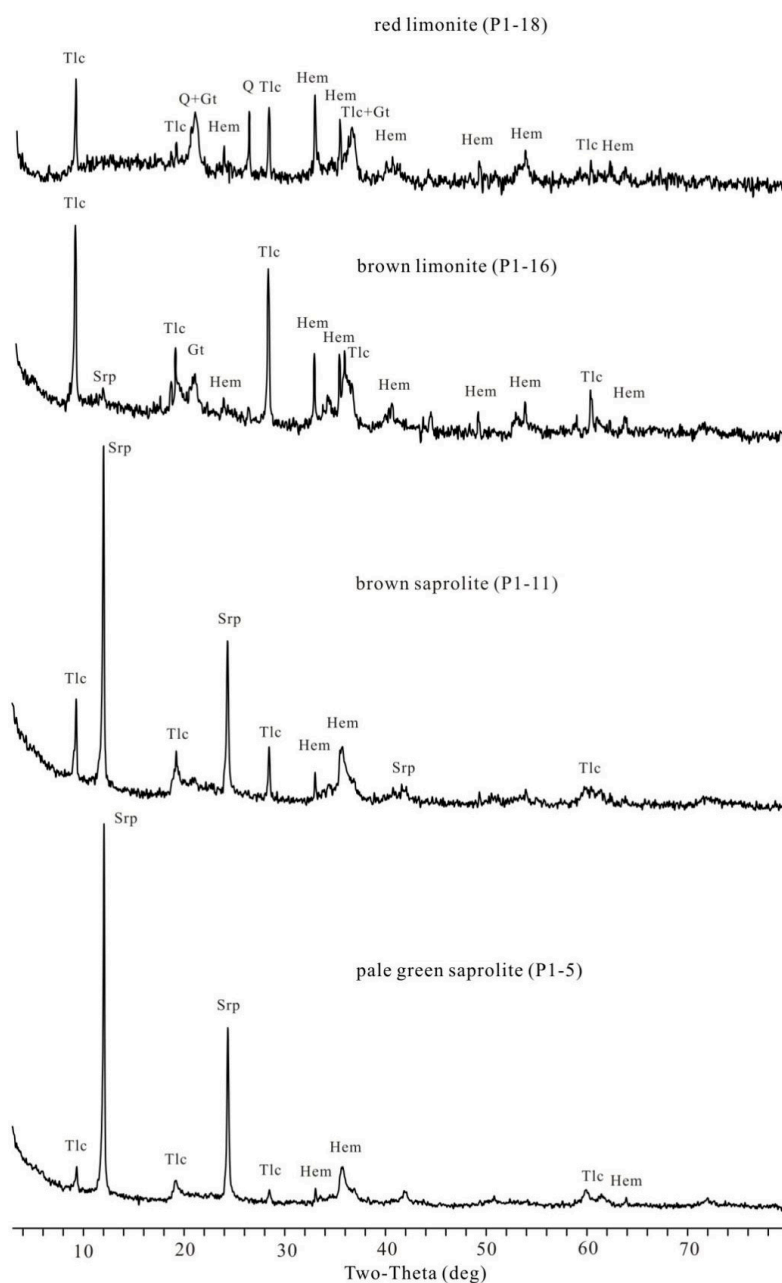


**Figure 6.** X-ray diffraction (XRD) patterns of the samples from different horizons in the Ni laterite profile. Abbreviations: Go, goethite; Hem, hematite; Srp, serpentine; Q, quartz; Px, pyroxene; Tlc, talc.

## 5.2. Whole-Rock Geochemistry

The analytical results of whole-rock samples are listed in Table 1, and representative data are graphically illustrated in Figure 7. Unweathered serpentinite is characterized by a high concentration of Mg (38.03 wt % MgO) and Si (38.8 wt % SiO<sub>2</sub>), coupled with low Fe (7.49 wt % Fe<sub>2</sub>O<sub>3</sub>) and Al (0.8 wt % Al<sub>2</sub>O<sub>3</sub>). It contains 0.18 wt % Ni, similar to ultramafic rocks associated with lateritic Ni deposits

elsewhere [6,15]. The saprolite samples have lower Mg (13.28–36.06 wt % MgO, mean 26.8 wt % MgO) and higher Fe (8.44–42.27 wt % Fe<sub>2</sub>O<sub>3</sub>, mean 20.28 wt % Fe<sub>2</sub>O<sub>3</sub>) and Al (0.76–2.49 wt % Al<sub>2</sub>O<sub>3</sub>, mean 1.43 wt % Al<sub>2</sub>O<sub>3</sub>) than the unweathered serpentinite. The contents of Ni range from 0.68 to 1.18 wt %, with an average of 1.03 wt %. Comparing the brown saprolite samples and the pale-green saprolite samples specifically, the former is characterized by a higher Fe and Ni concentrations but a lower Mg concentration than the latter. The limonitic samples exhibit a further decrease in Mg (mean 10.27% MgO) and Si (mean 28.82% SiO<sub>2</sub>) relative to the saprolite samples, but Fe (mean 44.0% Fe<sub>2</sub>O<sub>3</sub>) and Al mean 4.2% Al<sub>2</sub>O<sub>3</sub>) are significantly high. The Ni content of the limonite samples is ranging from 0.47 wt % to 0.59 wt %, with an average of 0.53 wt % Ni. The chemical difference between the red limonite sample and brown limonite sample within the limonite horizon is mainly demonstrated by the change of Si and Fe, and the red limonite have relatively higher Fe concentration but lower Si concentration than its brown analogs. In addition, the brown limonite is geochemically characterized by hosting the highest Mn concentration in all weathered samples. The alluvium sample show a significant high value of Si (41.05 wt % SiO<sub>2</sub>), which is consistent with the presence of quartz mentioned above, and it also contains abundant Fe (mean 20.45 wt % Fe<sub>2</sub>O<sub>3</sub>) and Al (mean 13.2 wt % Al<sub>2</sub>O<sub>3</sub>).

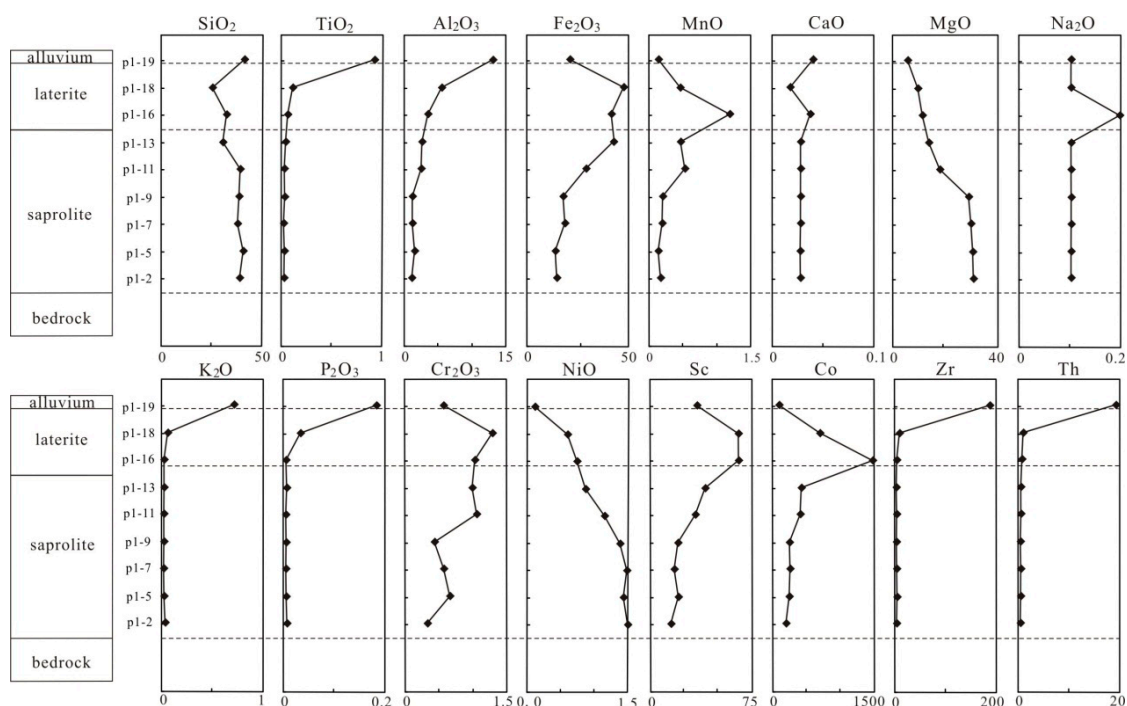


**Figure 7.** Variations of the major elements and selected trace elements with depth through the laterite profile with depth.

**Table 1.** Whole-rock analyses data of the samples from the Yuanjiang Ni laterite profile, including major element (wt %) and trace element (in mg/kg).

	Diluvial Horizon	Limonite Horizon			Saprolite Horizon					Bedrock	
	P <sub>1</sub> -19	Red Limonite P <sub>1</sub> -18	Brown Limonite P <sub>1</sub> -16	Brown Saprolite P <sub>1</sub> -13 P <sub>1</sub> -11		P <sub>1</sub> -9	P <sub>1</sub> -7	Pale green Saprolite P <sub>1</sub> -5 P <sub>1</sub> -2		J-3	J-1
SiO <sub>2</sub> (wt %)	41.05	25.76	31.87	29.65	39.08	38.83	37.62	40.29	38.88	39.23	38.80
TiO <sub>2</sub> (wt %)	0.89	0.08	0.04	0.02	0.01	0.01	0.002	0.01	0.01	0.03	0.002
Al <sub>2</sub> O <sub>3</sub> (wt %)	13.16	5.23	3.17	2.49	2.31	1.05	1.06	1.30	1.01	0.76	0.80
Fe <sub>2</sub> O <sub>3</sub> (wt %)	20.45	46.88	41.11	42.27	28.49	17.21	17.95	13.32	14.25	8.44	7.49
MnO (wt %)	0.13	0.44	1.17	0.46	0.51	0.18	0.18	0.13	0.15	0.08	0.05
MgO (wt %)	5.22	9.55	10.98	13.28	18.18	29.15	29.37	30.83	30.92	36.06	38.03
CaO (wt %)	0.04	0.02	0.04	0.03	0.03	0.03	0.03	0.03	0.03	0.03	0.05
Na <sub>2</sub> O (wt %)	0.1	0.1	0.2	0.1	0.1	0.1	0.1	0.1	0.1	0.1	0.1
K <sub>2</sub> O (wt %)	0.70	0.04	0.01	0.01	0.01	0.01	0.01	0.01	0.02	0.01	0.01
P <sub>2</sub> O <sub>5</sub> (wt %)	0.18	0.03	<0.01	<0.01	<0.01	<0.01	<0.01	<0.01	<0.01	<0.01	<0.01
LOI (wt %)	17.67	9.48	9.42	9.38	9.19	11.31	11.60	11.37	11.99	13.17	13.08
Cr (wt %)	0.36	0.88	0.69	0.67	0.71	0.29	0.38	0.44	0.22	0.36	0.30
Ni (wt %)	0.09	0.47	0.59	0.68	0.91	1.09	1.17	1.12	1.18	1.08	0.18
Sc (mg/kg)	34	63	65	40	33	20	17	20	15	9	8
V (mg/kg)	200	137	152	87	74	47	49	39	32	40	35
Co (mg/kg)	82	678	1493	409	391	231	242	229	185	92	100
Cu (mg/kg)	48	12	14	1	1	3	3	2	1	4	99
Zn (mg/kg)	117	199	188	122	90	54	75	57	32	46	32
Ga (mg/kg)	26	4	5	2	2	1	1	1	1	1	1
Ge (mg/kg)	3	1	2	2	1	2	2	2	1	1	1
Rb (mg/kg)	68	3	1	0.26	0.58	0.59	0.57	0.60	0.28	0.09	0.11
Sr (mg/kg)	57	4	2	1	1	1	1	1	1	1	2
Y (mg/kg)	20	3	5	26	14	4	0.31	0.30	0.15	0.11	0.11
Zr (mg/kg)	184	7	2	0.36	0.33	0.25	0.09	1	0.05	0.36	0.11
Nb (mg/kg)	18	1	0.38	0.14	0.12	0.09	0.08	0.18	0.06	0.06	0.06
Cs (mg/kg)	12	1	0.31	0.06	0.21	0.35	0.15	0.19	0.10	0.10	0.08
Ba (mg/kg)	168	15	37	60	100	31	26	19	21	5	5
Hf (mg/kg)	5	0.18	0.06	0.04	0.01	0.01	0.01	0.03	0.01	0.03	0.00
Ta (mg/kg)	1	0.06	0.03	0.01	0.01	0.02	0.01	0.06	0.00	0.01	0.01
Pb (mg/kg)	33	8	2	1	1	1	0.35	0.37	0.06	<0.01	2
Th (mg/kg)	19	1	0.23	0.01	0.02	0.02	0.02	0.07	0.00	<0.01	0.01
U (mg/kg)	4	0.22	0.07	<0.01	0.01	<0.01	<0.01	0.01	<0.01	<0.01	<0.01
Total	100.13	99.40	99.57	99.43	100.02	99.57	99.87	99.38	99.08	99.6	98.98
S/SAF	0.55	0.33	0.42	0.40	0.56	0.68	0.66	0.73	0.72	0.81	-
UMIA	42	60	51	51	35	21	22	17	18	11	10

Note: S/SAF = SiO<sub>2</sub>/(SiO<sub>2</sub> + Al<sub>2</sub>O<sub>3</sub> + Fe<sub>2</sub>O<sub>3</sub>); UMIA = 100 × [Al<sub>2</sub>O<sub>3</sub> + Fe<sub>2</sub>O<sub>3</sub>]/[SiO<sub>2</sub> + MgO + Al<sub>2</sub>O<sub>3</sub> + Fe<sub>2</sub>O<sub>3</sub>].



In general, the profile has a typical laterite geochemical pattern with an increase of Fe, Al, Mn and Ti but a decrease of Si and Mg upward from the bedrock. The concentration of Ni shows a trend of increasing in the saprolite horizon, reaching a maximum in the upper part of the saprolite horizon, and decreasing in the limonite horizon. Cobalt has the highest value (1493 mg/kg) in the limonite samples, and chromium shows its highest value (1.28 wt %) in the limonite sample as well. Although the concentrations of these residual elements in weathered products are several folds higher than that of the bedrock, none of them reached the level of economic significance.

### 5.3. Mineral Chemistry

Electron analysis results of selected minerals from various zones of the weathering profile are listed in Table 2. Serpentine from fresh serpentinite contains 0.09–0.21 wt % Ni. Similar Ni concentrations (0.16–0.21 wt %) are also observed in Talc. However, pyroxene has much lower Ni contents (0.03–0.07 wt %), indicating that elevated Ni in the lateritic weathering profiles is unlikely to originate from this mineral. Spinel also shows low Ni concentrations, which are mostly less than 0.1 wt % (not shown in Table 2).

Various minerals from the saprolite and limonitic zones have elevated Ni concentrations. Residual serpentine in the saprolite has a wide range of Ni from 0.34 to 1.2 wt %, with an average of 0.87 wt %, suggesting that the serpentine is the dominant Ni-bearing phase in the silicate ore of the Yuanjiang lateritic Ni deposit. In addition, the residual serpentine contains lower Mg and Si but higher Fe relative to the primary serpentine in the serpentinite, indicating that there is a chemical change during the weathering of serpentine. Residual talc has Ni (mean 0.21 wt % Ni) comparable with values of primary talc (mean 0.18 wt % Ni). This observation suggests that talc is not an important Ni host to the regolith, and the residual serpentine and talc were variably enriched in Ni during lateritization.

An unidentified mineral occurring as microfracture- or open void-infillings in saprolite is also observed (Figure 8b). This material is characterized by high Mn (14.2 wt %), Mg (17.74 wt %), Si (15.64 wt %) and Ni (2.47 wt %), being the most Ni-enriched phase in the Yuanjiang deposit. The EMPA results are broadly comparable to compositions of manganiferous wad (Ni-rich Mn-oxyhydroxides), but its specific mineralogical property remains unclear and needs further investigations.

With emphasis on the mode of Ni occurrence, some selected micro-areas from a saprolite sample were examined by elemental line scan and area scan mapping (Figure 8). Results show that Ni is heterogeneous in the residual serpentine of different generations. The vein-like and fibrous serpentines seem more Ni-enriched than those of flaky and tabular morphology (Figure 8a). Nickel and Mg are negatively correlated throughout the serpentine aggregates, whereas Ni and Fe are broadly positively correlated. Ni, Mn and Co is strongly enriched in manganiferous “wad” (Figure 8b).

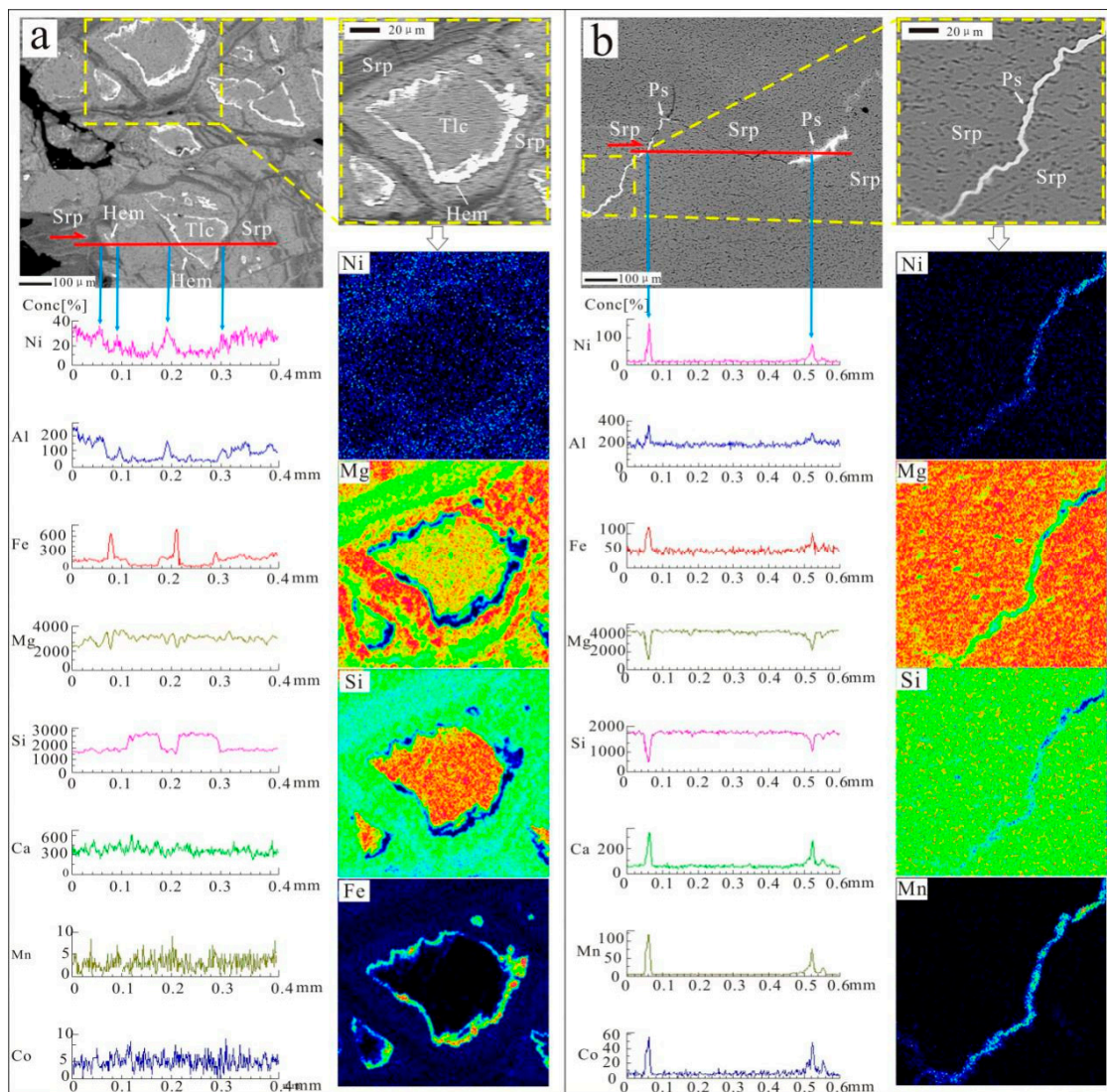


**Figure 8.** Element lines and mappings in some selected micro areas from the silicate ore at the saprolite: (a) elemental distribution in an aggregate of residual serpentines with different morphology; and (b) elemental distribution in a manganeseiferous “wad” appearing in a micro area.

**Table 2.** Electron microprobe analyses data of the primary and weathered minerals in the Yuanjiang Ni laterite profile (wt %).

	Minerals in the Bedrock						Minerals in the Saprolite					
	Primary Serpentine ( <i>n</i> = 5)		Pyroxene ( <i>n</i> = 4)		Primary Talc ( <i>n</i> = 3)		Weathered Serpentine ( <i>n</i> = 16)		Weathered Talc ( <i>n</i> = 3)		Unidentified Manganiferous Mineral ( <i>n</i> = 2)	
	Average	Range	Average	Range	Average	Range	Average	Range	Average	Range	Average	Range
SiO <sub>2</sub>	39.60	33.21–45.17	54.22	53.89–54.51	52.49	51.95–52.9	37.84	33.74–41.83	58.83	54.80–60.96	15.64	15.07–16.70
TiO <sub>2</sub>	0.03	0.00–0.07	0.08	0.00–0.18	0.05	0.00–0.08	0.05	0.00–0.16	0.02	0.00–0.06	0.11	0.04–0.20
Al <sub>2</sub> O <sub>3</sub>	1.73	0.32–4.05	3.20	2.21–4.02	0.14	0.12–0.17	2.40	0.32–5.22	0.17	0.10–0.28	2.88	2.82–2.95
Fe <sub>2</sub> O <sub>3</sub>	4.86	4.00–6.44	6.52	6.47–6.58	0.96	0.66–1.11	6.45	3.76–8.85	1.29	0.56–2.32	4.26	3.87–4.93
MnO	0.03	0.01–0.04	0.12	0.06–0.14	0.02	0.00–0.03	0.02	0.00–0.05	0.02	0.01–0.02	14.20	11.95–15.48
MgO	38.13	37.07–38.79	33.57	32.98–34.07	32.52	31.98–33.3	35.00	31.63–38.49	30.39	29.12–31.61	17.74	17.39–18.43
CaO	0.08	0.07–0.10	1.25	1.02–1.51	0.05	0.02–0.06	0.19	0.02–0.29	0.06	0.04–0.08	0.65	0.57–0.81
Na <sub>2</sub> O	0.00	0.00–0.00	0.02	0.00–0.04	0.04	0.01–0.07	0.02	0.00–0.03	0.01	0.00–0.02	0.44	0.09–1.14
K <sub>2</sub> O	0.01	0.00–0.02	0.01	0.00–0.02	0.04	0.03–0.05	0.02	0.00–0.06	0.01	0.00–0.02	0.04	0.02–0.06
Cr	0.21	0.00–0.49	0.44	0.4–0.46	0.12	0.05–0.2	0.74	0.12–1.57	0.1	0.1–0.1	0.06	0.02–0.12
Ni	0.16	0.09–0.21	0.05	0.03–0.07	0.18	0.16–0.21	0.87	0.34–1.20	0.21	0.18–0.26	2.47	2.15–2.92
Co	0.00	0.00–0.00	0.00	0.00–0.00	0.00	0.00–0.00	0.00	0.00–0.00	0.01	0.01–0.02	1.84	1.78–1.94



## 6. Discussions

### 6.1. Lateritization History

The chemical index of alteration (CIA,  $CIA = [Al_2O_3 / (Al_2O_3 + CaO^* + Na_2O + K_2O)] \times 100$  (%)) [43] is a widely used indicator for estimating the degree of weathering of rocks. This indicator, however, is not effective enough to reveal the weathering degree of our studied ultramafic rock since the rock of this type commonly contains low concentrations of CaO, Na<sub>2</sub>O and K<sub>2</sub>O. Thus, concerning the weathering of mafic or ultramafic rocks specifically, the S/SAF value ( $S/SAF = SiO_2 / (SiO_2 + Al_2O_3 + Fe_2O_3)$ ) [44], or the UMIA value (the ultramafic index of alteration,  $UMIA = 100 \times [(Al_2O_3 + Fe_2O_3) / (SiO_2 + MgO + Al_2O_3 + Fe_2O_3)]$ ) [20] might be better choices for the weathering degree evaluation, because MgO and SiO<sub>2</sub> tend to be leached out but Al<sub>2</sub>O<sub>3</sub> and Fe<sub>2</sub>O<sub>3</sub> are commonly enriched in the lateritic profiles. Applying the S/SAF index, we found that the regolith samples of Yuanjiang profile have an S/SAF value of 0.33–0.8. It is higher than other previously reported cases in modern rainforest condition. For instance, the Kolonodale lateritic Ni profile on Sulawesi Island, Indonesia, shows an S/SAF value ranging 0.04–0.66 [15]. In addition, in the SiO<sub>2</sub>–Al<sub>2</sub>O<sub>3</sub>–Fe<sub>2</sub>O<sub>3</sub> ternary diagram (Figure 9), the samples are plotted in the weak to moderate lateritization domain. Applying the UMIA index, the saprolite samples of this study have UMIA values in the range of 17–51 and limonite samples reach UMIA values up to 60, which is lower than those examples of strong weathered condition with UMIA values beyond 90, such as in Cuba and the Dominican Republic [20]. Hence, both the S/SAF and UMIA index indicate that the Yuanjiang lateritic Ni profile has experienced a not very strong lateritization process. This result is also corroborated by the geological and mineralogical characteristics of the profile. Specifically, the limonite horizon, which is an indication of strong lateritization process, is only developed with a thin thickness. Meanwhile, the Fe-oxyhydroxides, which reflect a mineral indicator of the strong lateritization process, are less abundant in the mineral compositions of the regolith samples. Thus, according to the above evidence, we speculate that the Yuanjiang profile is a product of weak to moderate level lateritization process. This relatively less intense lateritization degree of regolith may provide a possible explanation of why no garnierite ore was observed in Yuanjiang deposit, which is usually considered as a product of strong infiltration process under highly lateritization condition [15,24,45,46]. This situation of Yuanjiang deposit is similar to the Riddle deposit in Oregon, USA, where there is no significant garnierite-type mineralization within the Ni-bearing silicate zone either. Foose [39] addressed that it might be attributed to the relatively short weathering history.

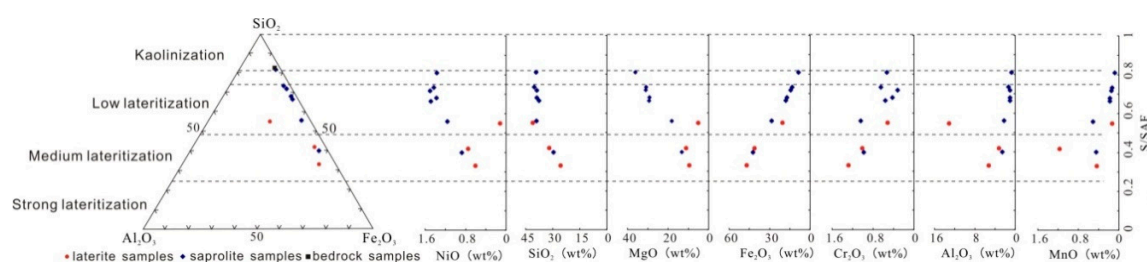


**Figure 9.** Lateritization degree of the Yuanjiang lateritic Ni profile and its relationship to element concentrations of different samples.

It is well accepted that the Ni laterite is principally regulated by climatic condition. Most Cenozoic lateritic Ni deposit are mainly distributed in a restricted latitude range of 22° N to 22° S, a zone dominated by tropical to subtropical climate [5]. It is further established that the lateritic Ni mineralization is particularly favored by warm (mean annual temperature of 19–29 °C) and humid (yearly precipitation of 1000–3200 mm) conditions [14]. Currently, the Yuanjiang district is located at 22.5° N latitude, with an average annual temperature of 21 °C and an average yearly precipitation of 1100 mm. Such a climatic condition is just at the margin of the “climate window” favoring the

lateritic weathering and associated Ni mineralization. Hence, the Ni laterite in Yuanjiang area is not the product of present climate environment alone but producer of its entire weathering history.

To answer when the lateritization began and how long it has lasted in Yuanjiang area is still a big challenge, since there is no reliable isotopic approach to constrain the history of the weathering of the ultramafic rocks. Previous work has depended on geological evidence to trace the lateritization history and understand the related climatic background. For example, there are many fossil lateritic Ni deposits along the Tethyan ophiolite belts, such as the Çaldag deposit in Turkey [11], Bitincke deposit in Albania [13] and those in Greece [47] and Oman [16], which are underlain sediments of known age. The stratigraphic relations thus provide indirect, minimum age constraints on lateralization and paleoclimatic conditions under which the lateritic Ni deposits formed. However, such stratigraphic correlations are lacking at Yuanjiang, and their formation ages remain undetermined. Thus, the climatic background and evolutionary history responsible for the formation of the Yuanjiang lateritic Ni deposit can only be inferred from some regional paleoclimatic proxies. The complete history of the Yuanjiang deposit can be traced to the late Triassic, when the ophiolites (the parent rock of the Yuanjiang deposit) were tectonically emplaced [30,31]. Unfortunately, the available paleoclimatic materials involving in the study site and regional areas are limited to a period from early Jurassic to present. Even so, the existing paleoclimatic materials from previous works may shed light to understand this issue.

Previous paleoclimatic studies show that, from the early Jurassic to late Cretaceous, the study area was characterized by arid to semi-arid subtropical climate with limited precipitation [48,49]. The aridity is well reflected by the widespread red beds containing abundant gypsum, halite, potash salt, mirabilite, and glauberite in many Jura-Cretaceous terrestrial basins in southwestern and southern China [49]. During this period, the climate condition was unconducive to the lateritization of ultramafic rocks. In late Oligocene, warm and humid climate emerged in south China, including the study area, as indicated by the presence of coal beds around the Oligocene-Miocene boundary in many terrestrial basins over the Yunnan Plateau [34]. Abundance of thick lignite deposits and oil shales in several Miocene to Pleistocene basins over the Yunnan Plateau confirms the prevalence of humid climates during the whole Neogene [34,50,51]. Well preserved fossil tropical–subtropical flora and fauna contained in some Miocene to Pliocene sediments provide additional evidence for humid climatic conditions [52–54]. Recent studies propose that the emergence of warm and humid climate in the Oligocene-Miocene boundary in the Yunnan Plateau has been genetically linked to the establishment of the Indian summer monsoon, which likely was due to significant uplift of the Tibet plateau at the same time [36,55–58]. The Indian summer monsoon must have brought abundant precipitation in SW China, which resulted in intense weathering and formation of the lateritic regolith. Supportive evidence includes the emergence of abundant supergene Mn deposits aged from 9.3 to 0.16 Ma in south China, particularly in Yunnan Province and adjacent Guangxi Province [36,59]. The formation of these supergene Mn deposits closely coincided with the intensification of the Indian summer monsoon [36], suggesting a causal link between lateritic weathering and the monsoonal climate. Thus, by inference, we speculate that the formation of the Yuanjiang lateritic Ni deposit might have a similar weathering timing and climatic background with those Neogene supergene Mn deposits. The humid climate conducive to lateritization of ultramafic rocks and supergene Ni enrichment in Yuanjiang area has probably prevailed since at least the late Miocene until the present. However, further geochronological work will hopefully provide precise age constraints on the lateritic Ni mineralization.

## 6.2. Impact of Tectonic Uplift

Large areas of the whole Yunnan Plateau are characterized by repeated uplift since the Pliocene [60,61], as indicated by the staged river incision and the stepped topography over this plateau. In the study area, the stepped topography is best illustrated by six-level denudation planes between 1700 and 2100 m on both sides of the Anding River. This suggests that the tectonic uplift in the Yuanjiang area and exerted a significant role in shaping the local geology and landscape.

The impact of tectonic uplift on weathering can be discerned from the occurrence of regolith profile. We notice that a thick saprolite horizon is stably developed within the serpentinite-derived regolith in study area, and it is usually thought to be controlled by the drainage condition in local hydrology [62]. Given the coupling of weathering and uplift time, uplift can enhance the relief, lower the water table and ultimately lead to the weathering front moving downward to deeper [3,21]. In addition, this tectonic-induced topographic change is considered to be conducive for enhancing recharge, infiltration, and reaction of groundwater [25]. It is probably the main reason a thick saprolite is the dominant unit of the regolith in study area. Conversely, tectonic uplift has also exerted a negative influence on regolith formation. It is thought to have promoted erosion, river incision, and subsequently result in the segmentation and thinning of the lateritic regolith [36]. The uplift- and river incision-induced erosion may explain a number of phenomena regarding to the field occurrence of regolith in Yuanjiang area, including the absence of lateritic Ni regolith at the highest elevations (VI-level planation surface), the isolation of weathering regolith on the stepped III-level and IV-level denudation planes, and the presence of only thin limonite horizon at the upper part of the regolith profile.

### 6.3. Mechanism of Ni Mineralization

To answer why Ni is enriched within the serpentinite-derived regolith in Yuanjiang area and explain the detailed mineralization features of this deposit, it is necessary to assess elemental behavior during lateralization. Numerous authors have mathematically used mass-balance calculations to estimate losses or gains of elements with the rock weathering, and various methods of the mass-balance calculation have been proposed. One possible choice is the chemical compositions based method [63–68], in which an immobile element selection is needed for normalization of compositions of the lateritic profiles [15,69,70]. However, in practical applications, discussion of which elements to use for mass balance calculations is commonly difficult. The other possible choice is the chemical compositions and physical properties integrative based method, in which the mass-balance calculation is expressed as a function of the constitutive relationships between the chemical compositions of parent and weathered material, their bulk densities, and volumes [42,71,72]. In this study, the parental rock structures are well preserved in the saprolite, which suggests that weathering processes have preserved the original volume [42]. Based on the assumption that the volume has not greatly varied between bedrock and saprolite, as well as the saprolite is the dominant unit of the profile, the volume mass-balance calculations can be applied. The net gains and losses of chemical constituents are calculated using the following equation [73]:

$$K_j = \left[ \left( \frac{C_{jw} \times \rho_{jw}}{C_{jp} \times \rho_{jp}} \right) - 1 \right] \times 100$$

where  $K_j$  is the gain and/or loss factor of chemical element  $j$ ;  $C_{jw}$  and  $C_{jp}$  are the concentrations of chemical element  $j$  in the weathered layer,  $w$ , and the parent material,  $p$ , respectively; and  $\rho_{jw}$  and  $\rho_{jp}$  are bulk densities of the weathered material,  $w$ , and the parent material,  $p$ , respectively.

As illustrated in Figure 10, many major elements (e.g., Mg, Si, Ca, Na and Cr) display an absolute loss throughout the profile. These elements tend to be most significantly depleted towards the upper zone of the lateritic profile (limonitic zone), with samples at base of the saprolite being least depleted. Over 60% of MgO ( $K_j = -60$ ) in the saprolite horizon, and even 89% of them were removed ( $K_j = -89$ ) in the limonite horizon. Silica is largely lost, with nearly 70% ( $K_j = -70$ ) in the limonite and nearly 36–63% ( $K_j = -36 \sim -63$ ) in the saprolite. Manganese concentration increases throughout the profile, notably in the lower part of the limonite and the upper part of the saprolite (Figure 10). This observation indicates that external Mn may have been introduced into the weathering profile by lateral flow of weathering solutions. The externally derived Mn may precipitate in joints and fractures of the weathered products as partly confirmed by the presence of manganiferous wad.



Nickel displays a slight loss in the red limonite ( $K_j = -10$ ), but begins to exhibit a marked gain in the brown limonite ( $K_j = +45$ ) and more significantly in the saprolite ( $K_j = +84 \sim +316$ ). This observation is consistent with several previously studied cases [15], and it can be explained by a well-accepted view that Ni is leached from the upper part of the profile and subsequently adsorbed in the lower part. The mobility of Ni, however, is complex and it may have various associations with the evolution of minerals, organic matter, pH environment and other factors during the lateritization. Nickel originated from the primary serpentine, which contains 0.09–0.21 wt % Ni. Pyroxene (0.03–0.07 wt % Ni) may have made a lesser contribution since they only account for a small proportion of the whole primary minerals. With the decomposition of these primary minerals, some Ni may have been leached in the first phase of weathering of serpentine and likely transported downward as bicarbonate or complexed with organic matters in weathering solutions [73–75].

After released from ultramafic parent rock to weathering solution, the mobility of Ni is to a great extent controlled by sorption, substitution and dissolution/precipitation processes, and the leached Ni can be fixed in various supergene minerals at different depths of a weathering profile [27,76–78]. In detail, at least three types of minerals were identified as the Ni-rich carriers and being responsible for the adsorption of Ni in the Yuanjiang profile. Firstly, in the upper part of the Yuanjiang lateritic profile, Ni was thought to be fixed in goethite due to its large surface area and open channel structure [79]. This view was confirmed by the XRF analytical results of the whole-rock samples in the limonitic zone, which is dominated by the goethite and hematite and have 0.6–1.2% Ni. Secondly, our EMPA analysis found a Ni-bearing manganiferous phase in the brown limonite sample with Ni concentrations up to 3.14 wt %, which suggest that Ni may be fixed to the manganiferous phase in some specific locations. However, this occurrence of Ni enrichment is relatively less as a whole. Notably, Ni could be expelled from goethite as it ages through successive dissolution and recrystallization cycles during the lateritization process [78], which promoted Ni migration downward to the lower part of regolith profile. In this position, part of the leached Ni may be fixed by silicate minerals based on the fact of high Ni concentration (0.34–1.2 wt % Ni) in the weathered serpentine. The  $\text{Ni}^{2+}$  in weathering solutions tend to substitute for  $\text{Mg}^{2+}$  in the structure of serpentine due to their similar ionic radius, particularly under alkaline conditions [64,76]. By means of Ni K-edge  $\mu\text{EXAFS}$ , it was confirmed that Ni was found in Ni–Mg and Ni–Ni mixed sites in Ni-bearing secondary serpentines [22]. Based on above observations and relevant knowledge, it is thus proposed that Ni mineralization in the Yuanjiang profile was mainly related to ion exchange reactions between the serpentine and weathering solution. In contrast, talc is not an active mineral for Ni ion exchange reaction in the saprolite horizon despite it is largely retained during the saprolitization. This view is supported by the low Ni concentration (0.18–0.26 wt % Ni) in the weathered talc of the silicate ore.

Besides Ni, Co is also worthy of attention for its potential economic significance in the laterite profile derived from the ultramafic rocks. Some lateritic Ni deposits contain significant amounts of Co that can be produced as a by-product. Examples include the Goro deposit in New Caledonia [10,80], Çalda deposit in Turkey [11] and Wingellina deposit in Australia [17]. At Yuanjiang, Co has a similar mobility behavior with Mn, as illustrated in Figure 10, owing to their geochemical affinity during the lateritization process [81–83]. Cobalt commonly preferentially enters the structure of low-crystallinity Mn-oxyhydroxydes by substitution in the lower part of the limonite horizon [8,12,17,84]. However, although some Co-bearing manganiferous “wad” (2 wt % Co) was occasionally identified in the studied elsewhere profile, whole-rock Co concentration maximum is only 0.15%, much lower than many Ni lateritic profiles such as Nkamouna profile in Cameroon (up to 0.84 wt % Co) [83] and Bulong profile in Australia (up to 2 wt % Co) [85]. The explanation of why Co mineralization is lacking in the Yuanjiang profile, firstly, may lie in the lower Co concentrations in the parent rocks, and, secondly, may be associated with the rare occurrence of Mn-oxyhydroxydes in the regolith, because Mn precipitation in regolith generally depends on late-stage mobility related to local drainage, geomorphology and other environmental conditions.

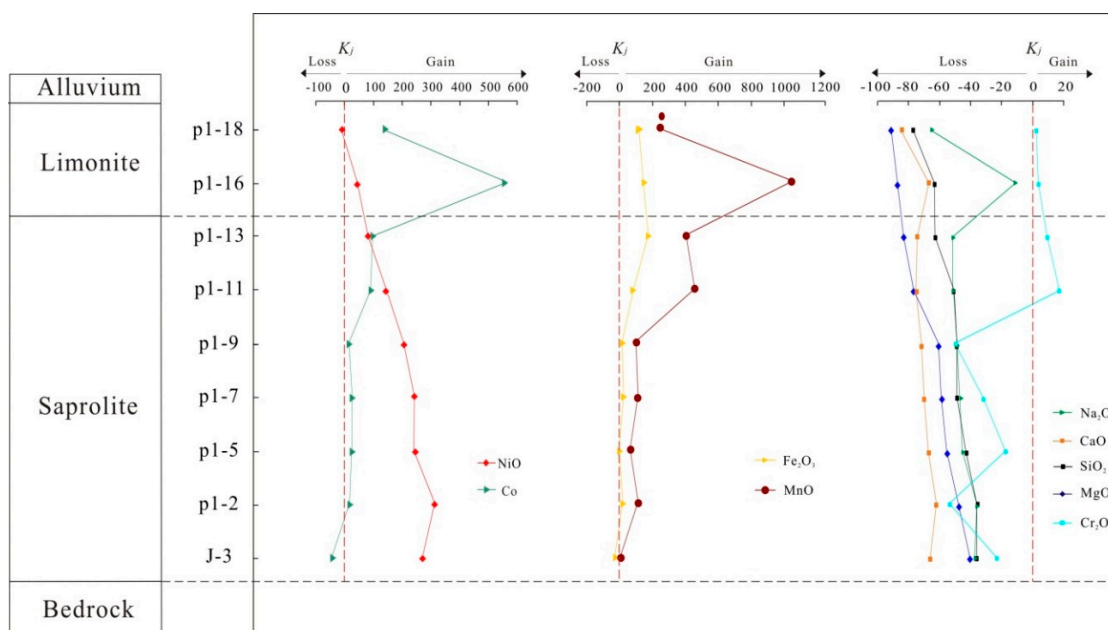


**Figure 10.** Results of the geochemical mass-balance calculations of some representative elements along the profile.

#### 6.4. Genetic Model for the Yuanjiang Lateritic Ni Deposit

Large accumulation of supergene Ni-rich minerals results from the interactions of oxidized meteoric waters with Ni-bearing precursor rocks under an optimum combination of lithological, climatic, and structural factors [4,5,7,21]. These factors contribute to the formation and preservation of the regolith in the region and to the development of the Yuanjiang Ni laterite deposit.

The Ni-bearing precursor rocks of Yuanjiang Ni deposit is linked to the Ailaoshan paleo-Tethyan ophiolites (Figure 11a). They are considered to be derived from the break-up of the Ailaoshan ocean basin in the early Carboniferous [32]. With the subduction and closure of the Ailaoshan ocean basin in late Triassic, fragments of the ophiolites were tectonically emplaced into the middle to late Triassic forming a mélangé along the Ailaoshan orogenic belt [30,31]. From the late Triassic to Cretaceous, the ophiolite remnants were greatly impacted by the Indosinian-Yanshanian orogenic thrust, and the ultramafic rocks within the ophiolite belt experienced multiple stages of deformation and metamorphism [32]. Large numbers of ultramafic bodies were compressed, fragmentized and even altered by syntectonic hydrothermal fluids [32]. The widely observed talc-veins filled in the serpentinite bodies in Yuanjiang area are speculated to have been formed at this time. Meanwhile, the ophiolite remnants probably outcropped at the surface at this orogenic time. Onset of the regional intense weathering of outcropped rocks may have started in the late Oligocene [34,36,51,59]. As discussed, the emergence of humid and warm climates linked to Indian monsoon resulted in the weathering of exposed rocks, and subsequently formed the thick lateritic regolith overlying ultramafic rocks in Yuanjiang area. Given the coupling of regional weathering and uplift time [36], the uplift contributed to the deepening of the regolith by impacting local hydrology on one the hand, while its periodic activity caused the isolation of regolith and raised them to different altitudes, forming the stepped distribution pattern, on the other hand.

The development of the Ni, mineralized regolith can be regarded as an advancement history of a weathering front moving from the surface to below the water table [21], coupled with Ni redistribution from the primary minerals of bedrock to the weathered minerals within regolith (Figure 11b). Lateral infiltration of water rich in dissolved Ni could also contribute to local enrichment of Ni down slope topography [26]. Weathering was preferentially developed in areas where joints and faults are most developed. The structurally enhanced permeability significantly promoted oxidation of bedrock to

form a ferruginous cover dominated by Fe-oxyhydroxydes at the surface of the ultramafic rocks [7,15], characterized by an increase in Fe and Al and a strong decrease in Mg, Si and Ca. Some  $\text{Ni}^{2+}$  released from the primary minerals is adsorbed by goethite at the limonite horizon, as at the Çaldağ deposit in Turkey [13]. Thus, the oxide ore (I-type) was formed firstly. As the weathering front moved to a deeper level, oxidation may have a weak influence on the lateritization, but the groundwater activities and rock–water interaction may play a more important role below the water table. Particularly, ion-exchange process between the phyllosilicate minerals and leached weathering solution may be prevailing [86]. Theoretically, the leached Ni in solution may tend to substitute for Mg in the structure of serpentine at alkaline conditions [21]. Therefore, the accumulation of Ni-rich silicate minerals at the saprolite horizon produced the silicate Ni ore (III-type), similar to the reports from Kolonodale deposit in Indonesia [15]. Regarding the oxide and silicate mixed ore (II-type), it represents the mineralogical and chemical transition between types I and III, and genetically it may be formed at a specific hydrological regime of water table fluctuations.

In summary, the Yuanjiang lateritic Ni deposit may have formed by the following scenarios: (1) development of Ailaoshan paleo-Tethyan ophiolites in early Carboniferous; (2) tectonic emplacement, deformation, metamorphism and exposure of the ophiolites remnants in late Triassic to Cretaceous; (3) weathering of ophiolites remnants and supergene Ni enrichment starting at least in late Oligocene under a humid subtropical climate; and (4) multi-stage lifting by syn-weathering period uplift and consequently segmentation of Ni laterite.

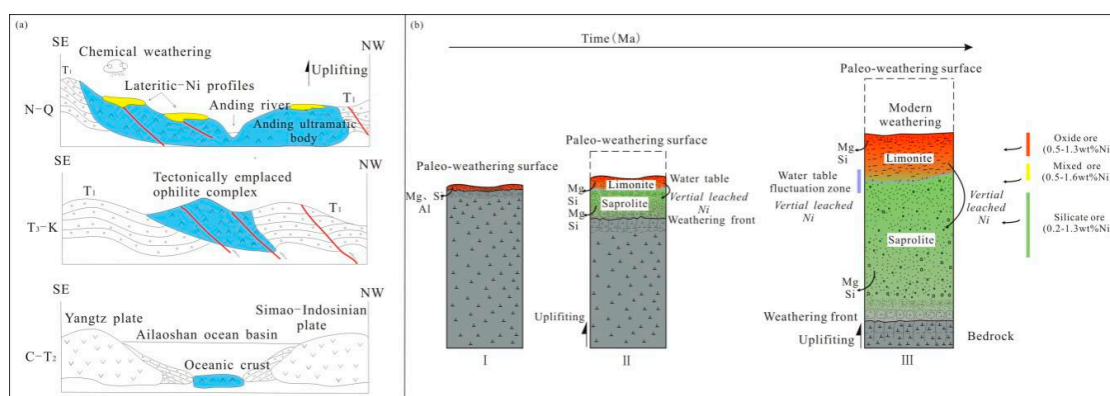


**Figure 11.** Formation and evolution history of the Yuanjiang lateritic Ni deposit. (a) A regional scale interpretation. C-T<sub>2</sub>: Development of the Ailaoshan paleo-Tethyan ophiolites; T<sub>3</sub>-K: Tectonic emplacement and exposure of the ophiolites remnants; N-Q: Weathering of the ophiolites remnants and formation of Ni laterite at the stepped landscape. (b) A profile scale interpretation. I: Oxidation of the bedrock and formation of the ferruginous cover. II: Differentiation of the limonite and saprolite with weathering front moved downward. Starting appearance of the oxide ore and mixed oxide-silicate ore. III: Deepening of each regolith unit impacted by tectonic uplifting and erosion of the upper part of the Ni laterite. The silicate ore was significantly formed at this stage.

## 7. Conclusions

The Yuanjiang lateritic Ni deposit can be classified as a silicate subtype with phyllosilicates and to a lower extent Fe-oxides as the main Ni-hosting phases. Compared to similar examples worldwide, it possesses similarities in profile geology and Ni-hosting minerals, but presents significant differences in ore types, especially lacking of the high grade garnierite ore. Three types of lateritic Ni ores (oxide ore, oxide-silicate mixed ore and silicate ore) are identified throughout the regolith profile, and it reflects the complex Ni redistribution history with serpentinite lateritization controlled by both mineral composition of parent rock and weathering environment. Ni is preferentially enriched in serpentine (0.34–1.2 wt % Ni) rather than talc (0.18–0.26 wt % Ni) despite their similarity in mineralogical nature.

Geochemical index (S/SAF and UMIA values) indicate that the studied serpentinite-derived Ni-rich regolith has experienced, at least, weak to moderate level lateritization that probably emerged at



the Oligocene-Miocene and continued to the present. Recent weathering is probably not lateritization, but is modifying the pre-existing lateritic regolith. The formation of the Yuanjiang lateritic Ni deposit is closely linked to regional multi-staged tectonic uplift during the development of Yunnan Plateau. This active tectonic setting has promoted weathering of serpentinite and supergene Ni enrichment, but is also responsible for its partial erosion.

**Author Contributions:** All authors contributed in a substantial way to the manuscript. W.F. conceived and designed the work that led to the submission, acquired data, and played an important role in interpreting the results. Y.F. contributed significantly to analysis and manuscript preparation. P.L. performed to analyse the data. Y.Z. performed the experiments. X.H. revised the manuscript. X.Z. contributed to field sampling work. Q.C. designed the experiments. Y.Z. helped perform the analysis with constructive discussions.

**Acknowledgments:** This research was financially supported by the National Natural Science Foundation (41462005) and the project of Collaborative Innovation Center for Exploration of Hidden Nonferrous Metal Deposits and Development of New Materials in Guangxi. We acknowledge the support of the Yuanjiang Nickel Mining Co., Ltd. for our field investigation. The authors also express gratitude to Hongyi Chen for his assistance with microprobe analysis at the Guilin University of Technology, and Jianlin Chen for his aid with bulk geochemical analysis at the Key Laboratory of Geochronology and Geochemistry, Chinese Academy of Sciences. This paper has also benefited greatly from comments and suggestions by Jianwei Li of China University of Geosciences. We appreciate careful and exhaustive comments and revisions of two anonymous journal reviewers, which improved the manuscript.

**Conflicts of Interest:** The authors declare no conflict of interests.

## References

1. Dalvi, A.D.; Bacon, W.G.; Osborne, R.C. *Past and future of nickel lateritic projects. International laterite Nickel Symposium, Perth, Australia, 28 September–1 October 2004*; Charlotte, N.C., Imrie, W.P., Lane, D.M., Eds.; TMS: Warrendale, PA, USA, 2004; pp. 23–50.
2. Berger, V.I.; Singer, D.A.; Bliss, J.D.; Moring, B.C. *Ni-Co Lateritic Deposits of the World—Database and Grade and Tonnage Models*; Open-File Report; U.S. Department of the Interior & U.S. Geological Survey: Reston, VA, USA, 2011; Volume 1058, pp. 1–26.
3. Butt, C.R.M.; Cluzel, D. Lateritic Nickel ore deposits: Weathered serpentinites. *Elements* **2013**, *9*, 123–128. [[CrossRef](#)]
4. Brand, N.W.; Butt, C.R.M.; Elias, M. Nickel lateritic: Classifications and features. *AGSO J. Aust. Geol. Geophys.* **1998**, *17*, 81–88.
5. Elias, M. *Nickel Lateritic Deposits—Geological Overview, Resources and Exploitation, in Giant Ore Deposit: Characteristics, Genesis and Exploration*; Special Publication; Centre for Ore Deposit Research, University of Tasmania: Tasmania, Australia, 2002; Volume 4, pp. 205–220.
6. Gleeson, S.A.; Herrington, R.J.; Durango, J.; Velázquez, C.A. The mineralogy and geochemistry of the Cerro Matoso S.A. Ni lateritic deposit, Montelibano, Colombia. *Econ. Geol.* **2004**, *99*, 1197–1213. [[CrossRef](#)]
7. Freyssinet, P.; Butt, C.R.M.; Morris, R.C. Ore-forming processes related to lateritic weathering. *Econ. Geol.* **2005**, 681–722.
8. Fouateu, R.Y.; Ghogomua, R.T.; Penaye, J.; Ekodecka, G.E.; Stendalc, H.; Colin, F. Nickel and cobalt distribution in the lateritics of the Lomié region, south-east Cameroon. *J. Afr. Earth Sci.* **2006**, *45*, 33–47. [[CrossRef](#)]
9. Lewis, J.F.; Draper, G.; Proenza, J.A.; Espaillet, J.; Jimenez, J. Ophiolite-Related Ultramafic Rocks (Serpentinites) in the Caribbean Region: A Review of their Occurrence, Composition, Origin, Emplacement and Ni-Lateritic Soils Formation. *Geol. Acta* **2006**, *4*, 237–263.
10. Wells, M.A.; Ramanaidou, E.R.; Verrall, M.; Tessarolo, C. Mineralogy and crystal chemistry of “garnierites” in the Goro lateritic nickel deposit, New Caledonia. *Eur. J. Miner.* **2009**, *21*, 467–483. [[CrossRef](#)]
11. Thorne, R.L.; Herrington, R.; Roberts, S. Composition and origin of the Çaldağ oxide nickel lateritic deposit, W. Turkey. *Miner. Depos.* **2009**, *44*, 581–595. [[CrossRef](#)]
12. Roqué-Rosell, J.; Mosselmans, J.F.W.; Proenza, J.A.; Labrador, M.; Galí, S.; Atkinson, K.D.; Quinn, P.D. Sorption of Ni by “lithiophorite–asbolane” intermediates in Moa Bay lateritic deposits, eastern Cuba. *Chem. Geol.* **2010**, *275*, 9–18. [[CrossRef](#)]

13. Thorne, R.; Roberts, S.; Herrington, R. The formation and evolution of the Bitincke nickel laterite deposit, Albania. *Miner. Depos.* **2012**, *47*, 933–947. [[CrossRef](#)]
14. Thorne, R.L.; Herrington, R.; Roberts, S. Climate change and the formation of nickel lateritic deposits. *Geology* **2012**, *40*, 331–334. [[CrossRef](#)]
15. Fu, W.; Yang, J.W.; Yang, M.L.; Pang, B.C.; Liu, X.J.; Niu, H.J.; Huang, X.R. Mineralogical and geochemical characteristic of a serpentinite-derived laterite profile from East Sulawesi, Indonesia: Implications for the lateritization process and Ni supergene enrichment in the tropical rainforest. *J. Asian Earth Sci.* **2014**, *93*, 74–88. [[CrossRef](#)]
16. Al-Khribash, S. Genesis and mineralogical classification of Ni-laterites. Oman Mountains. *Ore Geol. Rev.* **2015**, *65*, 199–212. [[CrossRef](#)]
17. Putzolu, F.; Balassone, G.; Boni, M.; Maczurad, M.; Mondillo, N.; Najorka, J. Mineralogical association and Ni-Co department in the Wingellina oxidetype laterite deposit (Western Australia). *Ore Geol. Rev.* **2018**, *97*, 21–34. [[CrossRef](#)]
18. Ratié, G.; Garnier, J.; Calmels, D.; Vantelon, D.; Guimaraes, E.; Monvoisin, G. Nickel distribution and isotopic fractionation in a Brazilian lateritic regolith: Coupling Ni isotopes and Ni K-edge XANES. *Geochim. Cosmochim. Acta* **2018**, *230*, 137–154. [[CrossRef](#)]
19. Mudd, G.M. Global trends and environmental issues in nickel mining: Sulfides versus laterities. *Ore Geol. Rev.* **2010**, *38*, 9–26. [[CrossRef](#)]
20. Aiglsperger, T.; Proenza, J.A.; Lewis, J.F. Critical metals (REE, Sc, PGE) in Ni laterites from Cuba and the Dominican Republic. *Ore Geol. Rev.* **2016**, *73*, 127–147.
21. Golightly, J.P. Progress in understanding the evolution of nickel laterites. In *The Challenge of Finding New Mineral Resources—Global Metallogeny, Innovative Exploration, and New Discoveries*; Goldfarb, R.J., Marsh, E.E., Monecke, T., Eds.; Society of Economic Geologists Special Publication; Society of Economic Geologists: Littleton, CO, USA, 2010; Volume 15, pp. 451–485.
22. Roqué-Rosell, J.; Villanova-De-Benavent, C.; Proenza, J.A. The accumulation of Ni in serpentines and garnierites from the Falcondo Ni-laterite deposit (Dominican Republic) elucidated by means of  $\mu$ XAS. *Geochim. Cosmochim. Acta* **2017**, *198*, 48–69. [[CrossRef](#)]
23. Fu, W.; Zhang, Y.M.; Pang, C.J.; Zeng, X.W.; Huang, X.R.; Yang, M.L.; Shao, Y.; Henry, L. Garnierite mineralization from a serpentinite-derived lateritic regolith, Sulawesi Island, Indonesia: Mineralogy, geochemistry and link to hydrologic flow regime. *J. Geochem. Explor.* **2018**, *188*, 240–256.
24. Villanova-de-Benavent, C.; Proenza, J.A.; Gali, S.; Garcia-Casco, A.; Tauler, E.; Lewis, J.F.; Longo, F. Garnierites and garnierites: Textures, mineralogy and geochemistry of garnierites in the Falcondo Ni-laterite deposit, Dominican Republic. *Ore Geol. Rev.* **2014**, *58*, 91–109. [[CrossRef](#)]
25. Ilyas, A.; Kashiwaya, K.; Koike, K. Ni grade distribution in laterite characterized from geostatistics, topography and the paleo-groundwater system in Sorowako, Indonesia. *J. Geochem. Explor.* **2016**, *165*, 174–188. [[CrossRef](#)]
26. Quesnel, B.; Veslud, C.L.C.D.; Boulvais, P.; Gautier, P.; Cathelineau, M.; Drouillet, M. 3D modeling of the laterites on top of the Koniambo Massif, New Caledonia: Refinement of the per descensum lateritic model for nickel mineralization. *Miner. Depos.* **2017**, *52*, 1–18. [[CrossRef](#)]
27. Myagkiy, A.; Truche, L.; Cathelineau, M.; Golfier, F. Revealing the conditions of Ni mineralization in the laterite profiles of New Caledonia: Insights from reactive geochemical  $\mu$ transport modelling. *Chem. Geol.* **2017**, *466*, 1–18. [[CrossRef](#)]
28. Qiao, F.G.; Zhu, J.Y.; Tian, Y.L. Nickel resources distribution in the World and nickel deposits in Yunnan Province, China. *Yunnan Geol.* **2005**, *24*, 95–401.
29. Wang, S.W.; Sun, X.M.; Liao, Z.W.; Qu, W.J.; Jiang, X.F.; Li, Y.C. Platinum group elements and Re-Os isotope geochemistry of harzburgites from Caiziyuan nickel deposit in Huili County of Sichuan Province and its geological significance. *Miner. Depos.* **2013**, *32*, 515–532.
30. Zhang, Q.; Zhou, D.J.; Li, X.Y.; Chen, Y.; Huang, Z.X.; Han, S.; Jia, X.Q.; Dong, J.Q. Characteristics and Geneses of Shuanggou Ophiolites, Yunnan Province, China. *Acta Petrol. Sin.* **1995**, *11*, 190–202.
31. Mo, X.X.; Pan, G.T. From Tethys to the formation of the Qinghai Tibet Plateau: Constrained by tectono magmatic events. *Earth Sci. Front.* **2006**, *6*, 43–51.
32. Liu, J.L.; Tang, Y.; Song, Z.J. The Ailaoshan Belt in Western Yunnan: Tectonic Framework and Tectonic Evolution. *J. Jilin Univ.* **2011**, *41*, 1285–1303.

33. Fang, W.X.; Hu, R.Z.; Xie, G.Q.; Su, W.C. Tectonolithostratigraphic units of the Ailaoshan area in Yunnan, China, and their implications of tectonic evolution. *Geotecton. Metall.* **2002**, *26*, 28–36.
34. Yunnan bureau of Geology and Mineral Exploration. *Regional Geology of Yunnan Province*; Geological Publishing House: Beijing, China, 1990.
35. Yin, A.; Harrison, T.M. Geologic evolution of the Himalaya-Tibetan orogen. *Annu. Rev. Earth Planet. Sci.* **2000**, *28*, 211–280. [[CrossRef](#)]
36. Deng, X.D.; Li, J.W.; Vasconcelos, P.M.; Cohen, B.E.; Kusky, T.M. Geochronology of the Baye Mn oxide deposit, southern Yunnan Plateau: Implications for the late Miocene to Pleistocene paleoclimatic conditions and topographic evolution. *Geochim. Cosmochim. Acta* **2014**, *139*, 227–247. [[CrossRef](#)]
37. Golightly, J.P. *Geology of Soroako nickeliferous lateritic deposits*, In *International Lateritic Symposium*, 2nd ed.; Evans, D.J.I., Shoemaker, R.S., Veltman, H., Eds.; AIME: New York, NY, USA, 1979; pp. 38–56.
38. Cluzel, D.; Vigier, B. Syntectonic Mobility of Supergene Nickel Ores of New Caledonia (Southwest Pacific). Evidence from Garnierite Veins and Faulted Regolith. *Resour. Geol.* **2008**, *58*, 161–170. [[CrossRef](#)]
39. Foose, M.P. *Nickel–Mineralogy and Chemical Composition of Some Nickel-Bearing Laterites in Southern Oregon and Northern California*; Bulletin; US Government Printing Office: Washington, DC, USA, 1992; pp. 1–24.
40. Sufriadin. *Mineralogy, Geochemistry, and Leaching Behavior of the Soroko Nickeliferous Laterite Deposits, Sulawesi, Indonesia*; Gadjah Mada University: Yogyakarta, Indonesia, 2013.
41. Tauler, E.; Proenza, J.; Gali, S.; Lewis, J.F.; Labrador, M.; Garcia-Romero, E.; Suarez, M.; Longo, F.; Bloise, G. Ni-sepiolite-falcondoite in garnierite mineralization from the Falcondo Ni-lateritic deposit, Dominican Republic. *Clay Miner.* **2009**, *44*, 435–454. [[CrossRef](#)]
42. Traoré, D.; Beauvais, A.; Chabaux, F.; Peiffert, C.; Parisot, J.C.; Ambrosi, J.P.; Colin, F. Chemical and physical transfers in an ultramafic rock weathering profile: Part 1. Supergene dissolution of Pt-bearing chromite. *Am. Miner.* **2008**, *93*, 22–30. [[CrossRef](#)]
43. Nesbitt, H.W.; Young, G.M. Early Proterozoic climates and plate motions inferred from major element geochemistry of lutites. *Nature* **1982**, *299*, 715–717. [[CrossRef](#)]
44. Hill, I.G.; Worden, R.H.; Meighan, I.G. Yttrium: The immobility-mobility transition during basaltic weathering. *Geology* **2000**, *28*, 923–926. [[CrossRef](#)]
45. Cathelineau, M.; Quesnel, B.; Gautier, P.; Boulvais, P.; Couteau, C.; Drouillet, M. Nickel dispersion and enrichment at the bottom of the regolith: Formation of pimelite target-like ores in rock block joints (Koniambo Ni deposit, New Caledonia). *Miner. Depos.* **2016**, *51*, 271–282. [[CrossRef](#)]
46. Fritsch, E.; Juillo, F.; Dublet, G.; Fonteneau, L.; Fandeur, D.; Martin, E.; Caner, L.; Auzende, A.L.; Grauby, O.; Beaufort, D. An alternative model for the formation of hydrous Mg/Ni layer silicates ('deweylite'/'garnierite') in faulted peridotites of New Caledonia: I. Texture and mineralogy of a paragenetic succession of silicate infillings. *Eur. J. Miner.* **2016**, *28*, 295–311. [[CrossRef](#)]
47. Skarpelis, N. Lateritization processes of ultramafic rocks in Cretaceous times: The fossil weathering crusts of mainland Greece. *J. Geochem. Explor.* **2006**, *88*, 1–3. [[CrossRef](#)]
48. Wang, H.Z.; Chu, X.C.; Liu, B.P. *Palaeogeography of China*; Map Publishing House: Beijing, China, 1985.
49. Liu, D.S.; Zheng, M.P.; Guo, Z.T. Initiation and evolution of the Asian monsoon system timely coupled with the ice-sheet growth and the tectonic movements in Asia. *Quat. Sci.* **1998**, *3*, 194–204.
50. Du, W.R. Geological characteristics and formation of the Tertiary lignite in Yunnan Province. *Yunnan Geol.* **1982**, *1*, 234–245.
51. Liu, R.X.; Xie, G.H.; Zhou, X.H.; Chen, W.J.; Fan, Q.H. Tectonic environments of Cenozoic volcanic rocks in China and characteristics of the source regions in the mantle. *Chin. J. Geochem.* **1995**, *14*, 289–302. [[CrossRef](#)]
52. Wang, S.J. Palaeoenvironmental change of the ancient Nihewan Lake area—Sr isotope evidence from Xiaodukou foraminifera. *Acta Geochim.* **1996**, *15*, 105–112.
53. Xu, J.X. Palynology, Paleovegetation and Paleoclimate of Neogene Central-Western Yunnan, China. Ph.D. Thesis, Graduate School of the Chinese Academy of Sciences, Shenzhen, China, 2003.
54. Wu, J.Y.; Sun, B.N.; Xie, S.P.; Lin, Z.C.; Yan, D.F.; Xiao, L. Two Neogene Machilus (Lauraceae) fossils leaves from Tengchong, Yunnan Province and its paleoenvironmental significance. *Geol. J. China Univ.* **2008**, *14*, 90–98.
55. Wang, P.X. Neogene stratigraphy and paleoenvironments of China. *Palaeogeogr. Palaeoclimatol. Palaeoecol.* **1990**, *77*, 315–334. [[CrossRef](#)]

56. Ding, Z.L.; Yu, Z.; Rutter, N.W.; Liu, T.S. Towards an orbital time scale for Chinese loess deposits. *Quat. Sci. Rev.* **1994**, *13*, 39–70. [[CrossRef](#)]
57. Clemens, S.C.; Murray, D.W.; Prell, W.L. Nonstationary phase of the Plio-Pleistocene Asian monsoon. *Science* **1996**, *274*, 943–948. [[CrossRef](#)]
58. Clift, P.D.; Hodges, K.V.; Heslop, D.; Hannigan, R.; Van Long, H.; Calves, G. Correlation of Himalayan exhumation rates and Asian monsoon intensity. *Nat. Geosci.* **2008**, *1*, 875–880. [[CrossRef](#)]
59. Li, J.W.; Vasconcelos, P.; Zhang, W.; Deng, X.D.; Duzgoren-Aydin, N.; Yan, D.R.; Zhang, J.Q.; Hu, M.A. Timing and duration of supergene mineralization at the Xinrong manganese deposit, western Guangdong Province, South China: Cryptomelane  $^{40}\text{Ar}/^{39}\text{Ar}$  dating. *Miner. Depos.* **2007**, *42*, 361–383. [[CrossRef](#)]
60. Jiang, F.C.; Wu, X.H. Late Cenozoic tectonic movement in geomorphologic boundary belt of southeastern Qinghai-Xizang Plateau. *J. Chengdu Univ. Technol.* **1998**, *25*, 162–168.
61. Guo, Z.T.; Yao, X.F.; Zhao, X.T.; Wei, L.Y. A tropical paleosol at high elevation in the Yulong Mountains and its implication on the uplift of the Tibetan Plateau. *Chin. Sci.* **2001**, *46*, 69–73. [[CrossRef](#)]
62. Anand, R.R.; Paine, M. Regolith geology of the Yilgarn Craton, Western Australia: Implications for exploration. *Aust. J. Earth Sci.* **2002**, *49*, 3–162. [[CrossRef](#)]
63. Grant, J.A. The isocon-diagram—A simple solution to Gresens' equation for metasomatic alteration. *Econ. Geol.* **1986**, *81*, 1976–1982. [[CrossRef](#)]
64. Burns, R.G. *Mineralogical Applications of Crystal Field Theory*; Cambridge University: Cambridge, UK, 1993; p. 551.
65. Baumgartner, L.P.; Olsen, S.N. A least square approach to mass transport calculations using the isocon method. *Econ. Geol.* **1995**, *90*, 1261–1270. [[CrossRef](#)]
66. Amundson, R. Soil formation. *Treatise Geochem.* **2003**, *5*, 1–35.
67. Brown, D.J.; Helmke, P.A.; Clayton, M.K. Robust geochemical indices for redox and weathering on a granitic lateritic landscape in Central Uganda. *Geochim. Cosmochim. Acta* **2003**, *67*, 2711–2723. [[CrossRef](#)]
68. Berger, A.; Frei, R. The fate of chromium during tropical weathering: A lateritic profile from Central Madagascar. *Geoderma* **2014**, *213*, 521–532. [[CrossRef](#)]
69. Ma, J.L.; Wei, G.J.; Xu, Y.G.; Long, W.G.; Sun, W.D. Mobilization and re-distribution of major and trace elements during extreme weathering of basalt in Hainan Island, South China. *Geochim. Cosmochim. Acta* **2007**, *71*, 3223–3237. [[CrossRef](#)]
70. Gong, Q.J.; Deng, J.; Yang, L.Q.; Zhang, J.; Wang, Q.F.; Zhang, G.X. Behavior of major and trace elements during weathering of sericite–quartz schist. *J. Asian Earth Sci.* **2011**, *42*, 1–13. [[CrossRef](#)]
71. Gresens, R.L. Composition-volume relations of metasomatism. *Chem. Geol.* **1967**, *2*, 47–65. [[CrossRef](#)]
72. Brimhall, G.H.; Dietrich, W.E. Constitutive mass-balance relations between chemical composition, volume, density, porosity and strain in metasomatic hydrochemical systems: Results on weathering and pedogenesis. *Geochim. Cosmochim. Acta* **1986**, *51*, 567–587. [[CrossRef](#)]
73. Barker, W.W.; Welch, S.A.; Banfield, J.F. Geomicrobiology: Interactions between microbes and minerals. In *Reviews in Mineralogy*, 2nd ed.; Banfield, J.F., Nealson, K.H., Eds.; Biogeochemical Weathering of Silicate Minerals; Mineralogical Society of America: Washington, DC, USA, 1997; Volume 35, pp. 391–428.
74. Gleeson, S.A.; Butt, C.R.M.; Elias, M. Nickel laterites: A review. *Econ. Geol.* **2003**, *4*, 12–18.
75. Retallack, G.J. Lateritization and bauxitization events. *Econ. Geol.* **2010**, *105*, 655–667. [[CrossRef](#)]
76. Golightly, J.P. Nickeliferous lateritic deposits. *Econ. Geol.* **1981**, *75*, 710–735.
77. Dublet, G.; Juillot, F.; Morin, G.; Fritsch, E.; Fandeur, D.; Ona-Nguema, G. Ni speciation in a new caledonian lateritic regolith: A quantitative x-ray absorption spectroscopy investigation. *Geochim. Cosmochim. Acta* **2012**, *95*, 119–133.
78. Dublet, G.; Juillot, F.; Morin, G. Goethite aging explains Ni depletion in upper units of ultramafic lateritic ores from New Caledonia. *Geochim. Cosmochim. Acta* **2015**, *160*, 1–15.
79. Carvalho-E-Silva, M.L.; Ramos, A.Y.; Tolentino, H.C.N.; Enzweiler, J.; Netto, S.M.; Alves, M.D.C.M. Incorporation of Ni into natural goethite: an investigation by X-ray absorption spectroscopy. *Am. Mineral.* **2003**, *88*, 876–882. [[CrossRef](#)]
80. Llorca, S.M. Metallogeny of supergene cobalt mineralization, New Caledonia. *Aust. J. Earth Sci.* **1993**, *40*, 377–38582.
81. Llorca, S.; Monchoux, P. Supergene cobalt minerals from New Caledonia. *Can. Miner.* **1991**, *29*, 149–161.



82. Lambiv, D.G.; Gleeson, S.A. Petrography, mineralogy, and geochemistry of the Nkamouna serpentinite: Implications for the formation of the Cobalt-Manganese Laterite Deposit, Southeast Cameroon. *Econ. Geol.* **2012**, *107*, 25–41.
83. Lambiv, D.G.; Gleeson, S.A.; Schofield, P.F. Mineralogical characterization of the Nkamouna Co–Mn lateritic ore, southeast Cameroon. *Miner. Depos.* **2013**, *48*, 155–171. [[CrossRef](#)]
84. Manceau, A.; Llorca, S.; Calas, G. Crystal chemistry of cobalt and nickel in lithiophorite and asbolane from New Caledonia. *Geochim. Cosmochim. Acta* **1987**, *51*, 105–113. [[CrossRef](#)]
85. Elias, M.; Donaldson, M.J.; Giorgetta, N. Geology, mineralogy, and chemistry of lateritic nickel-cobalt deposits near Kalgoorlie, Western Australia. *Econ. Geol.* **1981**, *76*, 1775–1783. [[CrossRef](#)]
86. Scott, K.M.; Pain, C.F. *Regolith Science*; CSIRO: Dordrecht, The Netherlands; Collingwood, Australia, 2008.



© 2019 by the authors. Licensee MDPI, Basel, Switzerland. This article is an open access article distributed under the terms and conditions of the Creative Commons Attribution (CC BY) license (<http://creativecommons.org/licenses/by/4.0/>).